Green Synthesis of Fe_2O_3 and Fe_3O_4 Nps Using *Calpurnia Aurea* LeafExtract and Its Application for Antibacterial Activity

By: Tahir Beshir Ketebo

A Thesis Submitted To the Department of Applied ChemistrySchool of Applied Natural Science

Presented in Partial Fulfillment of the Requirements for the Degreeof Master's in Chemistry (Industrial Chemistry)

Office of Graduate Studies

Adama Science and Technology University

Major Advisor: Fedlu Kedir (Phd)

Co - Advisor: Teshome Abdo (Phd)

May, 2024

Adama, Ethiopia

Green Synthesis of Fe_2O_3 and Fe_3O_4 Nps Using *Calpurnia Aurea* Leaf Extract and Its Application for Antibacterial Activity

By: Tahir Beshir Ketebo

Major Advisor: Fedlu Kedir (Phd)

Co - Advisor: Teshome Abdo (Phd)

A Thesis Submitted To the Department of Applied Chemistry

School of Applied Natural Science

Presented in Partial Fulfillment of the Requirements for the Degree of Master's in Chemistry (Industrial Chemistry)

Office of Graduate Studies Adama Science and Technology University

May 2024

Adama, Ethiopia

APPROVAL SHEET

To: Applied Chemistry Department

Subject: M.Sc Thesis Submission

This is to certify that the M.Sc thesis entitled "Green Synthesis of Fe_2O_3 and Fe_3O_4 Nps Using *Calpurnia Aurea Leaf* Extract and Its Application for Antibacterial Activity" submitted in partial fulfillment of the requirements for the degree of Master's in Science, the Graduate program of the department of Applied Chemistry, and has been carried out by Tahir Beshir Id. No PGE/18972/11, under my supervision. Therefore, I recommend that the student has fulfilled the requirements and hence hereby he can submit the thesis to the department.

Name of Student	Signature	Date
Name of major Advisor	Signature	Date
Co-advisor Signature Date	Signature	Date

Date of Submission _____

DECLARATION

I hereby declare that this Master Thesis entitled "Green Synthesis of Fe_2O_3 and Fe_3O_4 Nps Using *Calpurnia Aurea Leaf* Extract and Its Application for Antibacterial Activity" submitted to Adama Science and Technology University is my original work. That is, it has not been submitted for the award of any academic degree, diploma or certificate in any other university. All sources of materials that are used for this thesis have been duly acknowledged through citation.

Name of Student	Signature	Date

APPROVAL OF BOARD OF EVALUATORS

I the advisors of the thesis entitled "Green Synthesis of Fe_2O_3 and Fe_3O_4 Nps comparing Using *Calpurnia Aurea Leaf* Extract and Its Application for Antibacterial Activity" and developed by Tahir Beshir Ketebo here by certify that the recommendation and suggestions made by the board of examiners are appropriately incorporated into the final version of thethesis.

Name of major Advisor	Signature	Date

We, the under signed, members of the Board of Examiners of the thesis by Tahir Beshir Ketebo have read and evaluated the thesis entitled "Green Synthesis of of Fe_2O_3 and Fe_3O_4 Nps Using *Calpurnia Aurea Leaf* Extract and Its Application for Antibacterial Activity" and examined the candidate during open defense. This is, therefore, to certify that the thesis is accepted for partial fulfillment of the requirement of the degree of Master of Science in Industrial Chemistry.

Chairperson	Signature	Date
Internal Examiner	Signature	Date
External Examiner	Signature	Date

Final approval and acceptance of the thesis is contingent upon submission of its final copy to the Office of Postgraduate Studies (OPGS) through the Department Graduate Council (DGC) and School Graduate Committee (SGC).

Department Head	Signature	Date
School Dean	Signature	Date
Office of Postgraduate Studies	Dean Signature	Date

DEDICATION

This M.Sc thesis is dedicated to my beloved families whose advice, support and love helped me all along the right way and made me who I am today.

ACKNOWLEDGMENT

First of all I would like to thank the Allah, all praise to Allah for all his blessing in the completion of this thesis.

Next and foremost, I would like to express my genuine heart felt gratitude to my adviser Dr. Fedlu Kedir for his invaluable suggestion, comments, corrections, professional & technical guidance throughout my work for the successful accomplishment of this thesis.

Although I would like to express my deep gratitude to my Co-advisor, Dr. Tashome Abdo for his kind approach, invaluable suggestions, constructive comments and guidance throughout my thesis work.

I would like to acknowledge the department of Applied Chemistry for facilitating all the things to complete this research. I have also special thanks to chemistry laboratory lab assistances for their help during laboratory experiment and I would like to express my thanks to the department of Applied Biology for their help during UV visible spectroscopy and SEM analysis of laboratory work.

Finally I have special and deepest appreciations for my wife Hawa Gnaro Wakeyo who made me believe in myself and encouraged me through the whole process of research.

Contents

LIST OF TABLE

LIST OF FIGURE

LIST OF ABBREVIATION

DRS..... Diffuse reflectance spectroscopy

ROS…..... Reactive oxygen species

C. aurea..... *Calpurnia aurea*

C_B .....Conduction band

E_g.....Band gap energy

NP… ..... Nanoparticles

UV-Vis…..... Ultra violet visible

IONPs…..... Iron oxide nanoparticles

WHO.....World Health Organization

VB.....Valance band

XRD… .....X-Ray diffraction

P. aeruginosa .....*Pseudomonas Aeruginosa*

S. aureus… .....*Staphylococcus aureus*

E. coli .....*Escherichia Coli*

S. pyogenes… ..... *Streptococcus pyogenes*

ATCC.....American Type Culture Collection

DMSO…..... Dimethyl Sulfoxide

CFU…..... Colony Forming Unit

JCPDS…..... Joint Committee on Powder Diffraction Standards

ABSTRACT

Metal Oxide Nanoparticles have attained a great importance due to their unique properties. Among the metal oxide nanoparticles, Iron oxide is interesting because it has vast applications in various areas. In this study comparing iron oxide Fe_2O_3 and Fe_3O_4 nanoparticles. The Fe_2O_3 were synthesized by biogenic method using $FeCl_3.6H_2O$ and again Fe_3O_4 nanoparticles were synthesized by biogenic method using 1:2 ratios of ferrous sulphate hepta hydrate and ferric chloride hexa hydrate as precursory with the presence of C.aurea leaf extract in ratio of (2:1,1:2,1:1) for both of them . The synthesized nanoparticles were tested for antibacterial activity. The synthesized Fe_2O_3 and Fe_3O_4 nanoparticles were characterized by x-ray diffraction (XRD), scanning electron microscopy-energy, ultraviolet visible spectroscopy (uv-vis) and Fourier transformer infrared spectroscopy (FTIR). The crystal structure of nanoparticles were determined by XRD analysis the particle size of Fe_2O_3 nanoparticles 11.9,11.5 and 11.3nm for 2:1,1:2,1:1 ratio respectively and the particle size of Fe_3O_4 nanoparticles are 9.8,5.8 and 3.8nm for 2:1,1:2,1:1 ratio respectively. The DRS spectra investigation confirms the formation of Fe_2O_3 nanoparticles of the reflectance was exist at 200nm-850nm and for Fe_3O_4 nanoparticles 350nm-800 nm. Fourier transformer infrared spectroscopy study confirmed the presence of amines, carboxylic acids, phenols and alcohols. Generally, magnetite nanoparticles were found to be a better antibacterial activity compared to hematite nanoparticles. Among the magnetite nanoparticles ratios 1:1 Fe_3O_4 exhibited the highest inhibition zone against P. aeruginosa (10.34±0.47mm) at the concentration of 300mg/ml. The lowest zone of inhibition against E. coli and P. aeruginosa was observed at a concentration of 18.75 mg/ml (6.34 ± 0.47 mm) with mean and standard deviation respectively. In contrast, the highest zone of inhibition against S. aureus was observed with hematite 1:1 Fe_2O_3 at a concentration of 300 mg/ml (10.33 ± 0.47 mm) and the lowest at the concentration of 18.75mg/ml (6.33±0.47mm) for the S. pyogens.

Keywords: *Iron Oxide, Fe_3O_4, Fe_2O_3 Nanoparticles, Calpurnia aurea, Green Synthesis and antibacterial activity*

CHAPTER ONE

1. INTRODUCTION

1.1 Background

Nanotechnology can be defined as the manipulation of matter through certain chemical and physical processes to create materials with specific properties, which can be used in particular applications. A nanoparticle, a microscopic particle with at least one dimension less than 100 nanometers in size, forms the basis of this technology (Thakkar K.N et al., 2010). In principle, any collection of atoms bonded together with a structural radius of less than 100 nm can be considered a nanoparticle. Nanoparticles exhibit unique properties such as small size, narrow size distribution, low agglomeration, and high dispersion, bridging the gap between bulk materials and atomic or molecular structures. They possess distinct chemical and physical characteristics compared to bulk materials, including lower melting points, higher surface area, mechanical strength, specific optical properties, and magnetizations.

Nano materials find application across diverse fields such as cosmetics, paints, displays, batteries, medicine, catalysis, gas sensors, food engineering (production, processing, safety, and packaging), agriculture, energy (storage and conversion), and construction. In medicine, nanotechnology has been pivotal in addressing issues like antibiotic resistance in microorganisms. For instance, the synthesis of iron oxide (Fe_3O_4 and Fe_2O_3) nanoparticles has garnered significant attention due to their high specific surface area, facilitating interaction with bacterial surfaces and enhancing uptake by bacterial cells (Arivalagan.K et al., 2011).

Synthesis of nanoparticles can be achieved through various methods including chemical, physical, and biological approaches. Biosynthesis of nanoparticles, a green synthesis process, offers advantages over traditional chemical methods by producing metallic nanoparticles in a clean, nontoxic, and ecologically sound manner, without the need for high pressure, energy, temperature, or toxic chemicals (Ahmad.S et al., 2014).

Plant-mediated biological synthesis has emerged recently as a preferred method due to its ability to yield biocompatible nanoparticles suitable for biomedical applications, unlike chemical synthesis which may introduce toxic residues. (Fe_3O_4 and Fe_2O_3) nanoparticles synthesized

through green methods exhibit greater stability compared to those produced via chemical techniques, which can pose risks to human health and the environment (Laurent et al., 2008). This stability and biocompatibility make them ideal candidates for applications requiring antibacterial properties (Abdullah et al., 2020). The use of Calpurnia aurea leaf extract for the green synthesis of (Fe_3O_4 and Fe_2O_3) nanoparticles highlights its potential in producing eco-friendly materials with antibacterial activity. Calpurnia aurea, known for its medicinal properties against various ailments, including bacterial dermatitis, has been traditionally used in treatments owing to its antibacterial and antioxidant properties (Yineger H et al., 2008). In this study, the antibacterial activity of these eco-friendly nanoparticles synthesized from Calpurnia aurea leaf extract is investigated against common bacterial strains including gram-negative (Escherichia coli, Pseudomonas aeruginosa) and gram-positive bacteria (Staphylococcus aureus, Streptococcus pyogenes). This research aims to compare their effectiveness with conventionally synthesized (Fe_3O_4 and Fe_2O_3) nanoparticles for similar applications, emphasizing the potential of green synthesis in nanotechnology for sustainable biomedical and environmental solutions.

1.2. Statement of the Problem

Bacterial infections are major contributors to morbidity and have become increasingly difficult to manage due to the emergence of antimicrobial resistance. The prevalence of antibiotic resistance and multi drug resistant strains Gram +ve and Gram −ve microbes a serious threat to global population. Such resistance is due to indiscriminate use of antibiotics favoring evolution of novel antibiotic resistance strains at faster pace. (Raghunath A and Perumal , 2017) The World Health Organization (WHO) highlighted one of the most common causes of death in the world due to microbial contamination and pathogens resistance to drugs (Sportelli et al., 2016).Therefore synthesis of new and effective antimicrobial agents seems to be of greater importance. Recent advances in the field of nanotechnology bolster the ability to prepare metal oxide nano particles (NPs) of specific size and shape which contribute to the development of new antibacterial agents. Advantage of nano materials over traditional antibiotics is due to their surface area and chemical reactivity is exceedingly large as compared to bulk materials. Therefore, Fe_2O_3 and Fe_3O_4 nanoparticles are attracting much attention in the field of biomedicines either as contrast agents for, heating mediators for hyperthermia, drug delivery carriers and antimicrobial agents (Azam et al., 2012). NPs have shown broad-spectrum antibacterial activities against Gram $_+$ve and Gram $_-$ve bacteria because metal NPs have the ability to change the metabolic activity of bacteria (Chatzimitakos et al., 2016).*Calpurnia aurea* is commonly known as in Amharic „**Digita'** and in Oromic **'Cheka'** Ethiopia. The name Digita is used in several ways in Ethiopia. It can indicate the tree of this leaf is used in our area for tapeworm, fungus, gastric ache, ameba, rabies and it dry the wound. In the same area, the plant is traditionally used to treat rheumatism (Yineger H et al., 2008). Antibacterial and antioxidant activity of *C. aurea (Calpurnia aurea)* will have been reported (Adedapo.A et al., 2008), and the plant has been used to treat bacterial dermatitis (Tadeg.H et al., 2005).This evidences about the medicinal values of this plant, the present study would be used leaf extract of *Calpurnia aurea* for green synthesis of eco-friendly Fe_2O_3 and Fe_3O_4 nanoparticles for the study of antibacterial activity against gram negative *(Escherichia coli), (Pseudomonas aeruginosa)* and gram positive bacteria *(Staphylococcus aureus),(Streptococcus pyogenes).*This is to compare with Fe_2O_3 and Fe_3O_4 nanoparticles that would be synthesized by green method for the same application.

1.3. Objective of the Study

1.3.1. General objective

To synthesize Fe_2O_3 and Fe_3O_4 nanoparticles using the leaf extract of "Cekata or Degita"*Calpurnia aurea* plant (green method) and for application of antibacterial activity.

1.3.2. Specific objectives

- To synthesize Fe_2O_3 and Fe_3O_4 nanoparticles using *Calpurnia aurea* leaf extract and precursor salts, and characterize them with XRD, SEM, FT-IR, and UV/Vis spectroscopy techniques.
- To evaluate antibacterial activity of Fe_2O_3 and Fe_3O_4 nanoparticles *Staphylococcus aureus*, *Streptococcus pyogenes* and *Escherichia coli, Pseudomonas aeruginosa.*
- To compare the antibacterial activity of Fe_2O_3 and Fe_3O_4 nanoparticles

1.4 Significance of the study

Calpurnia aurea, known for its natural antioxidant and antimicrobial properties, treats various ailments in humans and animals. It aids in amoebic dysentery, diarrhea, head lice, ticks, syphilis, leishmaniasis, tapeworm, trachoma, Tinea capitis, wounds, scabies, elephantiasis, and swellings (M.Getachew, 2020). Green synthesis methods using *Calpurnia aurea* leaf extract for Fe_2O_3 and Fe_3O_4 nanoparticles offer a sustainable approach for antibacterial applications. This study benefits future researchers and promotes further exploration of *Calpurnia aurea's* potential.

1.5 Scope/delimitation of the study

The study on the green synthesis of Fe_2O_3 and Fe_3O_4 nanoparticles using *Calpurnia aurea* leaf extract is limited to using the extract as a reducing and stabilizing agent. The antibacterial activity will be tested against selected bacterial strains. The research will not address the long-term stability of the nanoparticles or their environmental impact.

CHAPTER TWO

2. LITERATURE REVIEW

Nanotechnology is one of the most significant emerging sciences of the 21st century, with rapid global growth in research and development. Among its key products are metallic nanoparticles, which are defined as particles less than 100 nm in size. These nanoparticles are prized for their unique optical, catalytic, electrical, and magnetic properties (Ankamwar et al., 2005). Nanotechnology has profoundly impacted various scientific fields, producing numerous products in biology and medicine, such as reducing the side effects of chemotherapy drugs (Arap W et al., 1998).

Additionally, nanotechnology addresses critical challenges in microbiology, particularly antibiotic-resistant microorganisms. Traditional organic disinfectants have several drawbacks, including toxicity to humans and instability under extreme industrial conditions. Consequently, there is increasing interest in inorganic disinfectants like metal oxides, which exhibit strong antimicrobial activity at low concentrations and are stable in harsh conditions. These compounds are often non-toxic and sometimes contain essential minerals (Gordon et al., 2011). Metal oxide nanoparticles effectively inhibit different bacterial strains, with their activity depending on whether the bacteria are gram-positive or gram-negative, reflecting differences in their cell walls (Hajipour et al., 2012).

Transition metal and metal oxide nanoparticles also serve as efficient heterogeneous and homogeneous catalysts in organic transformations, due to their participation in acid-base and redox reactions. These nanoparticles possess high surface-to-volume ratios, act as reusable heterogeneous catalysts, and enhance reaction rates. Moreover, oxidation reactions occur at surface oxygen atoms. When metal oxides are immobilized, magnetic separation of catalysts from reaction mixtures becomes more energy-efficient (using a magnetic field).

Nanoparticles are classified based on dimensionality, composition, shape, and origin. Dimensional classification includes zero-dimensional nanoparticles like quantum dots, one-dimensional nanoparticles such as nanowires and nanotubes, two-dimensional nanoparticles like nanofilms and nano sheets, and three-dimensional nanostructured bulk materials, including nano composites and nano porous materials. Compositionally, nanoparticles are divided into organic, inorganic, and hybrid types.

Organic nanoparticles are carbon-based, including dendrimers, micelles, and liposomes, while inorganic nanoparticles are made from metals (e.g., gold, silver), metal oxides (e.g., TiO_2, ZnO), and semiconductors (e.g., silicon, cadmium selenide). Hybrid nanoparticles combine organic and inorganic components, such as core-shell structures with metallic cores and polymeric shells. Shape-based classification includes spherical nanoparticles, like colloidal gold, rod-shaped nanoparticles, like nanorods, and platelet-like structures, such as graphene sheets. Origin classification differentiates natural nanoparticles (e.g., volcanic ash) from engineered nanoparticles created for specific purposes (e.g., carbon nanotubes, quantum dots), and incidental nanoparticles produced as industrial byproducts (e.g., combustion-generated particles). This comprehensive classification supports the targeted design and application of nanoparticles, ensuring their effective and safe use in technological advancements.

2.1. Iron oxides

In the past decade, the synthesis of magnetic IONPs has been intensively developed not only for its fundamental scientific interest but also for its many technological applications, such as targeted drug delivery, magnetic resonance imaging (MRI), magnetic hyperthermia and thermo ablation, bio-separation, and bio-sensing (Yang L et al., 2008). Particularly, bio applications based on magnetic nanoparticles (NPs) have received considerable attention because NPs offer unique advantages over other materials. For example, magnetic IONPs are inexpensive to produce, physically and chemically stable, biocompatible, and environmentally safe.

Eight iron oxides are known, among these iron oxides, hematite (α-Fe_2O_3), magnetite (Fe_3O_4) and maghemite (γ-Fe_2O_3) are very promising and popular candidates due to their polymorphism involving temperature-induced phase transition. Each of these three iron oxides has unique biochemical, magnetic, catalytic, and other properties which provide suitability for specific technical and biomedical applications (Cornell and Schwertmann., 2003.

Hematite (α-Fe_2O_3) as the most stable iron oxide and n-type semiconductor under ambient conditions, hematite (α- Fe_2O_3) is widely used in catalysts, pigments and gas sensors due to its low cost and high resistance to corrosion. It can also be used as a starting material for the synthesis of magnetite (Fe_3O_4) and maghemite (γ-Fe_2O_3), which have been intensively pursued for both fundamental scientific interests and technological applications in the last few decades (Wu et al., 2010). Hematite is an n-type semiconductor with a band gap of 2.3 eV, where the conduction band (CB) is composed of empty d-orbitals of Fe^{3+} and the

valence band (VB) consists of occupied 3d crystal field orbitals of Fe^{3+} with some admixture from the O 2p non- bonding orbitals (Zhang et al., 1993). As shown in figure 1(a), Fe^{3+} ions occupy two-thirds of the octahedral sites that are confined by the nearly ideal hexagonal close-packed O lattice.

Maghemite (γ-Fe_2O_3) as shown in figure 1(c), the structure of γ-Fe_2O_3 is cubic; each unit of maghemite contains 32 O^{2-} ions, 21⅓ Fe^{3+} ions and 2⅓ vacancies. Oxygen anions give rise to a cubic close-packed array while ferric ions are distributed over tetrahedral sites (eight Fe ions per unit cell) and octahedral sites (the remaining Fe ions and vacancies). Therefore, the maghemite can be considered as fully oxidized magnetite, and it is an n-type semiconductor with a bandgap of 2.0 eV.

Magnetite (Fe_3O_4) as shown in figure 1(b), Fe_3O_4 has the face centered cubic spinel structure, based on 32 O^{2-} ions and close-packed along the direction. Fe_3O_4 differs from most other iron oxides in that it contains both divalent and trivalent iron. Fe_3O_4 has a cubic inverse spinel structure that consists of a cubic close packed array of oxide ions, where all of the Fe^{2+} ions occupy half of the octahedral sites and the Fe^{3+} are split evenly across the remaining octahedral sites and the tetrahedral sites. In stoichiometric magnetite Fe^{II}/Fe^{III} = 1/2, and the divalent irons may be partly or fully replaced by other divalent ions (Co, Mn, Zn, etc). Thus, Fe_3O_4 can be both an n- and p-type semiconductor. However, Fe_3O_4 has the lowest resistivity among iron oxides due to its small bandgap (0.1 eV) (Boxall et al., 1996).

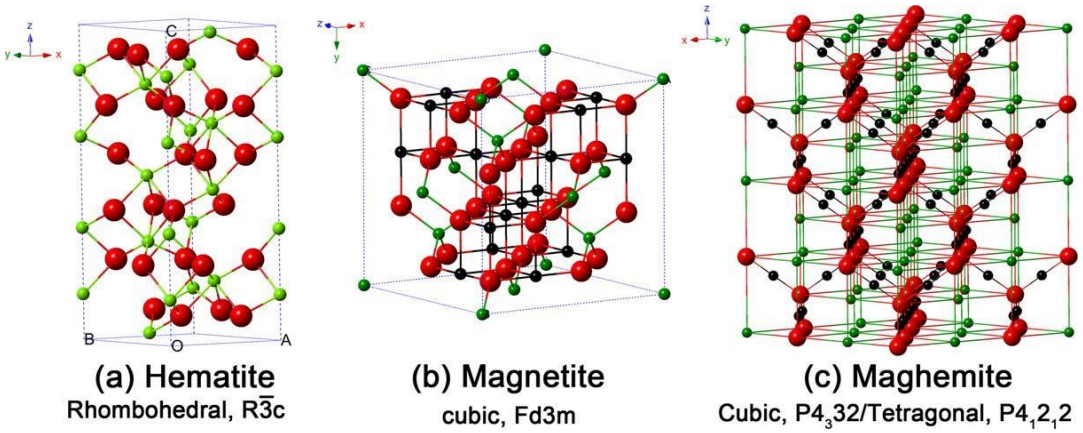

Figure 1: Crystal structure and crystallographic data of the hematite, magnetite and maghemite(the black ball is $Fe^{2+,}$ the green ball is Fe^{3+} and the red ball is O^2. (Gogoi et al., 2022)

2.2 Iron Oxide (Fe_2O_3) Nano particles

Iron oxide nanoparticles are amongst the most used for incorporation in wastewater treatment catalysts (Chen et al., 2009). Iron oxide nanoparticles has found great attention in the catalysis and adsorbent chemistry due to its unique properties, such as extremely small size, surface modifiability, high surface-area-to-volume ratio, great biocompatibility and excellent magnetic properties (Xu.P et al., 2012). For these unique properties it has found applications in gene therapy, targeted drug delivery, biochemical sensing, ultra-sensitive disease detection, high throughput genetic screening, and rapid toxicity cleansing (Gu et al., 2006)

Iron oxide nanoparticles have been incorporated in composites either as a core or a shell and in other cases as alloys (Harraz et al., 2014). IONP (Iron oxide nano particles) has antibacterial activity at relatively very high concentrations. The activity can be further moderate by changing the surface potential and accessible surface functional groups (Gudkov.S et al., 2021). The changes cause change in interaction pattern at the nano-bio interface, hence play crucial role in determining the antimicrobial propensity of IONPs. However, the enhance production of ROS because of the interaction potential at the interface is the principal cause for antimicrobial propensity of the NPs (Arakha et al., 2015).

2.3 Iron Oxide Fe_3O_4 Nanoparticles

Magnetic nanoparticles possess significant novel phenomena like super Para magnetism, high field irreversibility, high saturation field, extra anisotropy contributions or shifted loops after field cooling. These phenomena are due to the finite size and surface effects that control the magnetic behavior of individual nanoparticles. So these groups of nanoparticles have been used in the field of biotechnology, biomedicine, material science, engineering and environmental areas (Tartaj et al., 2003). In this context, magnetic nano-materials, such as iron oxide, magnetite (Fe_3O_4) have been applied in various fields such as drug carriers and contrast agents in magnetic resonance imaging.

Fe_3O_4 nanoparticles have attracted intensive research interest because of their important applications in cancer therapy, drug delivery, magnetic resonance imaging (MRI) and wastewater treatment (Vicky et al., 2010). Because of low cost, availability and properties possessed are similar to that of other metallic nanoparticles and other applications include heat transfer systems as super strong materials, sensors, antimicrobial, bactericidal agents used to coat hospital equipment and also as catalysts.

Controlling size and size distribution during synthesis is crucial for managing properties like superparamagnetism and hyperthermia in Fe_3O_4 nanoparticles. These nanoparticles exhibit different behaviors under an external magnetic field based on their size, with significant changes in magnetic properties occurring when reduced from micrometer to nanometer scale. (Figuerola et al., 2010).

2.4 Synthesis of Fe_2O_3 and Fe_3O_4 Nanoparticles

The manufacture of nanoparticles can be broadly defined into two approaches. The first is the top down approach and involves a material undergoing significant size reduction via physical processes. During size reduction, the resulting particle size, shape, and surface structure are heavily dependent on the technique used. Unfortunately, size reduction also tends to introduce surface imperfections that can significantly impact the overall physicochemical properties of the fabricated nanoparticle.

The second, bottom up approach builds nanoparticles via the assembly of atoms, molecules, and smaller particles or monomers (Cheng et al., 2013). There are three main routes for the synthesis of Fe_2O_3 and Fe_3O_4 Nps chemical, physical and biological. These have been investigated in order to produce more stable, soluble, biocompatible, and shape and size-controlled nanoparticles (Jiang et al., 2008).

2.5. Properties of Fe_2O_3 and Fe_3O_4 Nanoparticles

Due to their size (diameters ranging from 1 to 100 nm) nanoparticles present specific and controllable properties that are different from those they present on the macroscopic scale thus enabling unique applications (Yetter et al., 2009). It is known that the ratio between the number of surface atoms and the number of massive atoms increases significantly with particle size reduction (Chang et al., 2023). As the surface atoms have less coordination in relation to massive atoms, nanostructured materials exhibit significantly different physical, chemical, optical, mechanical, electrical and also magnetic properties. The excess of energy of surface atoms contributes for many of the extraordinary characteristics of nanoparticles (Campos E.A et al., 2015). This way, nanoscale materials present great potential for applications in several technological areas such as nano electronics and computer technology, medicine, aeronautics and space exploration, biotechnology and agriculture (Malik.S et al., 2023) The Conducted a study on the influence of iron nanoparticles in the shell of iron oxide Fe_2O_3, which converts to Fe_3O_4 when heated, on the microstructure and properties of hardened and tempered steel. The

modification of iron nanoparticles in the shell of Fe_3O_4 oxide led to the dispersion of the sub grain structure and a decrease in crystal lattice parameters of solid solutions. The injection of iron nanoparticles into the steel melt before crystallization resulted in improved mechanical properties, with higher yield, tensile strengths, and toughness compared to the original steel. The optimal improvement mode was found to be quenching at 900 °C and tempering at 550 °C. (Liu et al., 2021) introduced a mesoporous magnetic nano-system for the delivery of a pigenin, focusing on its antitumor mechanism. The study did not directly address the properties of Fe_3O_4 and Fe_2O_3 nanoparticles but highlighted the potential applications of magnetic nano composites in drug delivery systems. The magnetic properties of Fe_3O_4 and Fe_2O_3 nanoparticles can be controlled by specific molar ratios of reactants during synthesis Additionally, the synthesis of tailored magnetite (Fe_3O_4) and maghemite ($\gamma-Fe_2O_3$) nanoparticles using energetic electron assistance was investigated, emphasizing the structure and magnetic properties of the nanoparticles (Energetic Electron-Assisted Synthesis of Tailored Magnetite (Fe_3O_4) and Maghemite ($\gamma-Fe_2O_3$) Overall, the literature suggests that Fe_3O_4 and Fe_2O_3 nanoparticles have unique properties that can be influenced by synthesis methods and can be utilized in various applications, including drug delivery (Kurczewska.J and Dobosz.B, 2024) systems and material science. Further research is needed to explore the full potential of these nanoparticles in different fields.

2.5.1. Magnetic Properties

Iron (III) oxide, or Fe_2O_3, commonly known as rust, exhibits interesting magnetic properties (Nguyen M.D et al., 2021). At room temperature, it is antiferromagnetic, meaning its magnetic moments align in a regular pattern but in opposite directions within adjacent unit cells, resulting in a net magnetic moment of zero. This arrangement makes Fe_2O_3 non-magnetic in the conventional sense, as it doesn't exhibit any significant magnetic attraction (Fang.Q et al., 2011). However, under certain conditions, such as at low temperatures or when subjected to a strong magnetic field, Fe_2O_3 can become weakly ferromagnetic. This means that the antiferromagnetic arrangement can be disrupted, and the material exhibits a weak magnetization in the direction of the applied magnetic field. The magnetic properties of Fe_2O_3 have important implications in various fields, including materials science, geology, and environmental science. Understanding its behavior under different conditions is crucial for applications such as magnetic storage

devices, magnetic resonance imaging (MRI), and magnetic nanoparticles used in biomedical applications (Materon et al., 2021). Magnetic phenomena at the atomic scale were discovered in the early twentieth century, whereas the discovery of the first known magnetic material, Fe_3O_4, revolutionized the field of magnetism. The magnetic properties of a material depend on temperature, the applied magnetic field, and pressure. A change in these variables will result in the existence of two or more forms of magnetism. Ferro- and ferrimagnetic materials like Fe_3O_4 and some of their alloys have particles whose shape is asymmetrical when they are obtained by the grinding of bulk materials. Depending on the procedure used to form particles, they can be crystalline or amorphous spherical in shape. To a large extent, the synthesis process determines the degree of impurities in a particle, as well as the presence of structural defects, and, hence, the division of these defects inside the particle structure can be used to discover its magnetic properties (Chung et al., 2004).Magnetization depends on the number of unpaired valence electrons present in the atoms of solids and on the relative orientations of the neighboring magnetic moments. Two types of motion of electrons in atoms are responsible for magnetism. One is the spin of electrons around the atom‟s axis, and the other is the motion of electrons in an orbit around the nucleus (Duan and Guojun, 2005).

2.5.2 Structural Properties

These different crystal structures result in variations in the physical and chemical properties of Fe_2O_3. For example, hematite is often found as a red-brown mineral, maghemite can vary in color from brownish to black, and magnetite is typically black in color. Additionally, these variations in structure can affect properties such as magnetic behavior, electrical conductivity, and reactivity with other substances. Magnetite‟s crystal structure follows an inverse spinel pattern with alternating octahedral and tetrahedral-octahedra layers (Hill et al., 1979). Ferrous species are observed to occupy half of the octahedral lattice sites due to greater ferrous crystal field stabilization energy (CFSE); alternatively, ferric species occupy the other octahedral lattice sites and all tetrahedral lattice sites.

2.5.3 Physical Properties

The physical properties of hematite and magnetite nanoparticles (NPs) have been extensively studied in recent literature. (Hjiri et al., 2024) synthesized hematite NPs using sol-gel and Pechini sol-gel techniques, resulting in different morphologies and gas sensing performances.

The H material exhibited ellipsoid-shaped particles, while the H material had peanut-shaped particles with open pores and channels, leading to enhanced gas adsorption and diffusion. The size of NPs also plays a crucial role in gas sensing performance, with smaller crystallite sizes increasing surface area and sensitivity.

Additionally, magnetite NPs have been investigated for their magnetic, chemical, and crystallographic properties during microbial reduction processes Composite materials combining hematite and magnetite have been explored for photo catalytic degradation applications Furthermore, the influence of magnetite and its weathering product, maghemite, on NPs interactions and properties has been studied.

Natural and synthesized magnetite micro-scale crystals exhibit metallic luster and opaque jet black color, Magnetite‟s density is established at 5.18 g/cm3, slightly lighter than reddish-brown hematite (α-Fe_2O_3; 5.26 g/cm3) and somewhat heavier than yellowish orange ferrihydrite (α-FeOOH; 4.26 g/cm3); pure iron (α-Fe) has a density of 7.87 g/cm3. At ambient temperatures, magnetite particles exhibit hardness of 5.5, identical to glass. Magnetite particles are not porous. Standard Gibb‟s free energy of magnetite formation is -1012.6 kJ/ mol; therefore, formation of magnetite is thermodynamically favorable (Cornell and Schwertmann, 2003). Additionally, the standard enthalpy and entropy of magnetite formation are -1115.7 kJ/mol and 146.1 kJ/mol/K, respectively Overall, the synthesis methods, morphologies, and sizes of hematite and magnetite NPs significantly impact their physical properties and potential applications in various fields.

2.5.4 Chemical Properties

Iron (III) oxide (Fe_2O_3) nanoparticles possess unique chemical properties due to their small size and high surface area-to-volume ratio. These properties can include enhanced reactivity, catalytic activity, and magnetic behavior compared to bulk materials. Additionally, Fe_2O_3 nanoparticles may exhibit altered optical, electronic, and magnetic properties, making them valuable in various applications such as catalysis, biomedicine, and environmental remediation.

Fe_3O_4 nano materials have great importance because of their magnetic properties and wide applications. The investigation of Fe_3O_4 NPs in biological and material sciences is booming in recent times because of their various chemical and physical properties. They exhibit multiple potential applications, including magnetic fluid, magnetic micro-device, MRI, magnetic hyperthermia, water purification, and drug delivery. Significant size dependent structural and

optical properties of colloidal iron and iron oxide NPs correspond to electrical structure and quantum size effects of NPs. The respective synthesis method can affect their size and crystal structure as well (Estelrich et al., 2015). Chemically, Fe_3O_4 NPs are very active and can easily be oxidized in air, generally resulting in the loss of dispersibility and magnetism. Thus, it is important to keep the stability of magnetic Fe_3O_4 NPs by developing some effective protection strategies and providing proper surface coating (or grafting) with organic molecules, polymers, surfactants, biomolecules, or inorganic layer such as silica, metal, metal sulfide, metal oxide, or nonmetal elementary substances (Zhou et al., 2009).

2.6. Techniques of synthesis of metal oxide Nano particles

2.6.1. Sol-gel method

The sol-gel process is a wet-chemical technique that uses either a chemical solution (sol short for solution) or colloidal particles (sol for Nano scale particle) to produce on an integrated network gel (Navio et al., 2010).Metal alkoxides and metal chloride are typical precursors. They undergo hydrolysis and poly condensation reactions to form a colloid,system composed of nano particles dispersed in a solvent.The sol evolves then towards the formation of an in organic continuous network containing a liquid phase (gel). Formation of a metal oxide involves connecting the metal centers with oxo (M-O-M) bridges, therefore generating metal-oxo or metal hydroxo polymers in solution. After a drying process, the liquid phase is removed from the gel. Then, a thermal treatment (Calcinations) may be performed in order to favor further poly condensation and enhance mechanical properties. This is shown in figure 2.

Figure 2: Sol-gel method processing (Ganachari et al., 2019)

2.6.2. Precipitation method

The precipitation method is one of the most common methods for synthesizing nano materials. In the precipitation method, substances with different chemical components are mixed, and a precipitant is added to obtain a precursor precipitate (Hossein.P et al., 2015). The precursor precipitate is then dried or calcined to produce the corresponding nanoparticles. .When the particle diameter is about 1 μm, a precipitate is formed. The particle size of the particles generally depends on the solubility of the precipitate and the super saturation degree of the solution. The smaller the solubility of the precipitate is, the smaller the diameter of the particle produces, and the smaller the super saturation degree of the solution is, the larger the diameter of the particle forms (Arpan.B et al., 2015). The photo catalyst prepared by the precipitation method has good light absorption capability and can promote the separation of holes, and it can there by improve photo catalytic performance. In the precipitation process, many of the heavy metals added do not readily react in solution and may introduce impurities into the solution, which limits the application of the precipitation method. During the operation of the precipitation method, the reaction temperature, time, pH value, ratio of reactants, titration rate, and other factors have a certain influence on the material preparation. The precipitation method shows the characteristics of low cost, simple process, and safety (Lee et al., 2020).

2.6.3. Green synthesis method

The biological method, which is represented as an alternative to chemical and physical methods, provides an environmentally friendly way of synthesizing nanoparticles. Moreover, this method does not require expensive, harmful and toxic chemicals (Gebreslassie.Y et al., 2023). Metallic nanoparticles with various shapes, sizes, contents and physicochemical properties can be synthesized thanks to the biological method actively used in recent years. Synthesis can be done in one step using biological organisms such as bacteria, action bacteria, yeasts, molds, algae and plants, or their products. Molecules in plants and microorganisms, such as proteins, enzymes, phenolic compounds, amines, alkaloids and pigments perform nanoparticle synthesis by reduction (Shah M et al., 2015). In traditional chemical and physical methods; reducing agents involved in the reduction of metal ions, and stabilizing agents used to prevent undesired agglomeration of the produced nanoparticles carry a risk of toxicity to the environment and to the cell. Besides, the contents of the produced nanoparticles are thought to be toxic in terms of

shape, size and surface chemistry. In the green synthesis method in which nanoparticles with biocompatibility are produced, these agents are naturally present in the employed biological organisms. Plants, which have great potential for detoxification, reduction and accumulation of metals, are promising, fast and economical in removing organic pollutants (Rafael.A et al., 2023). Metallic nanoparticles having various morphological characteristics can be produced intra cellularly and extra cellularly. Synthesis process; is initiated by addition of extracts obtained from plant parts such as leaves, roots, stem and fruits into the aqueous solution of metal ions. With the materials present in the plant extract, such as sugar, flavonoid, protein, enzyme, polymer and organic acid, acting as a reducing agent, takes charge in bio induction of metal ions into nanoparticles (Iravani .S et al., 2011).Generally, the synthesis of iron oxides by green synthesis is the most convenient, easy, environmentally friendly way and minimizes the side effects of chemical and physical methods by preventing the use of toxic chemicals and formation of harmful/dangerous by-products.

2.7. Applications of Nano particles

2.7.1. For Antimicrobial Activity

Antibacterial agents considerably help to prevent and treat infectious diseases in humans and animals; however, the increase of resistant bacterial strains has turned to a serious challenge in medicine. Nano materials have attracted the researchers‟ interest due to their significant antibacterial activity. Antibiotics have been a mainstay of human health. They have been extensively used in clinics to treat respiratory tract infections, urinary tract infections, gastrointestinal infections and infections of nervous system (Singh et al., 2014).

Nanoparticles have a high specific surface area, so they are able to interact with bacterial surface structures. Furthermore, because of their relatively small size, they can facilitate the particle uptake by bacterial cells (Hufschmid et al., 2015). NPs-based biomedical applications have received considerable attention due to their ease of laboratory synthesis, cost effectiveness, physical and chemical stability, as well as biocompatibility and environmental safety (Hui et al., 2008). Consequently, Fe_2O_3 and Fe_3O_4 nanoparticles could be viable options for their potential application in antibacterial treatment.

2.7.2 Methods for Anti-bacterial Activity Test

Evaluating anti-bacterial activity is crucial for developing new antibiotics and disinfectants. Various methods are employed to determine the effectiveness of substances against bacterial strains, ensuring their suitability for medical and industrial applications. The most known and basic methods are the disk-diffusion and broth or agar dilution methods (Balouiri.M et al., 2016).

Disk diffusion refers to the diffusion of an antimicrobial agent of a specified concentration from disks, into the solid culture medium that has been seeded with the selected inoculum isolated in a pure culture. Disk diffusion is based on the determination of an inhibition zone proportional to the bacterial susceptibility to the antimicrobial present in the disk (Gajic et al., 2022). The diffusion of the antimicrobial agent into the seeded culture media results in a gradient of the antimicrobial. When the concentration of the antimicrobial becomes so diluted that it can no longer inhibit the growth of the test bacterium, the zone of inhibition is demarcated. The diameter of this zone of inhibition around the antimicrobial disk is related to minimum inhibitory concentration (MIC) for that particular bacterium/antimicrobial combination; the zone of inhibition correlates inversely with the MIC of the test bacterium. Generally, the larger the zone of inhibition, the lower the concentration of antimicrobial required to inhibit the growth of the organisms. Disk-diffusion assay offers many advantages over other methods simplicity, low cost, the ability to test enormous numbers of microorganisms and antimicrobial agents, and the ease to interpret results provided (Jeffrey et al., 2008).

Dilution methods are the most appropriate ones for the determination of MIC values, since they offer the possibility to estimate the concentration of the tested antimicrobial agent in the agar (agar dilution) or broth medium (macro dilution or micro-dilution). Either broth or agar dilution method may be used to quantitatively measure the invitro antimicrobial activity against bacteria and fungi. MIC value recorded is defined as the lowest concentration of the assayed antimicrobial agent that inhibits the visible growth of the microorganism tested, and it is usually expressed in mg/mL or mg/L.There are many approved guidelines for dilution antimicrobial susceptibility testing of fastidious or non-fastidious bacteria (Faller et al., 2004).

Broth dilution method: Broth micro- or macro-dilution is one of the most basic anti microbial susceptibility testing methods. Broth di1ution is a technique in which containers ho1ding identical volumes of broth with antimicrobia1 so1ution in incrementally (usua11y geometrica11y) increasing concentrations are inocu1ated with a known number of bacteria. It involves preparing two-fold dilutions of the antimicrobial agent in a liquid growth medium dispensed in tubes containing a minimum volume of macro dilution or with smaller volumes micro dilution. The MIC is the lowest concentration of antimicrobial agent that completely inhibits growth of the organism in tubes or micro dilution wells as detected by the unaided eye. The agar dilution method involves the incorporation of varying desired concentrations of the antimicrobial agent into an agar medium (molten agar medium), habitually using serial two-fold dilutions, followed by the inoculation of a defined microbial inoculum onto the agar plate surface. The MIC endpoint is recorded as the lowest concentration of antimicrobial agent that completely inhibits growth under suitable incubation conditions. This technique is suitable for both antibacterial and antifungal susceptibility testing. If multiple isolates are being tested against a single compound, or if the compound (or extract) tested masks the detection of microbial growth in the liquid medium with its coloring, agar dilution method is often preferred to broth dilution for the MIC determination (Yamamoto et al., 2001). In this studies disk diffusion method was used for anti bacterial activity.

2.7.3. Anti-bacterial Mechanism of Fe_2O_3 and Fe_3O_4 Nanoparticles

The antimicrobial mechanisms of NPs involve three model oxidative stress induction, metal ion release, or non-oxidative mechanism. The advantage of the NPs is that these three mechanisms can occur simultaneously (Wang.L et al., 2017). Subsequently, NPs damage the basic components of the bacterial cell such as DNA, lysosomes, ribosomes, enzyme inhibition, proteins deactivation, changes in cell membrane permeability, and changes in genes expression that ultimately leads to cell death (Xu *et al*., 2016). So, there is dire need to focus on biocompatible NP-based material with antibacterial activity.

Due to difference in the cell walls of Gram +ve and Gram −ve the action of NPs dependent on bacterial strains (Tran *et al*., 2010). The mechanism involves electrostatic interaction between bacterial cell wall and NPs which deteriorate cell wall of bacteria and induces toxic oxidative stress by producing reactive oxygen species (Ahmad.S et al., 2014).

The bactericidal effects of Fe_2O_3 andFe_3O_4 NPs provide high bioactivity even if small dose is used. Contrarily, the action of antibiotics attacks three bacterial sites that is, Cell wall, translational machinery and DNA replication, due to this reason bacterial resistance develop against each one of these modes of actions (Woolhouse et al., 2015). The modes of action of NPs develop a direct contact with the bacterial cell wall that damages the bacterial cell without penetration to the cell. Therefore, NPs are less prone to bacterial resistance than antibiotics (Wang *et al*., 2017). Biocompatibility of Fe_2O_3 and Fe_3O_4 NPs make it promising material against every type of pathogens (Li .Y et al., 2012). In addition, positive surface charge of the metal NPs promote their binding to the negatively charge surface of bacteria which enhance antimicrobial activity of Fe_2O_3 and Fe_3O_4 NPs (Seil and Webster, 2012).Figure3 shows the detail mechanism of iron oxide nanoparticles against bacterial cells.

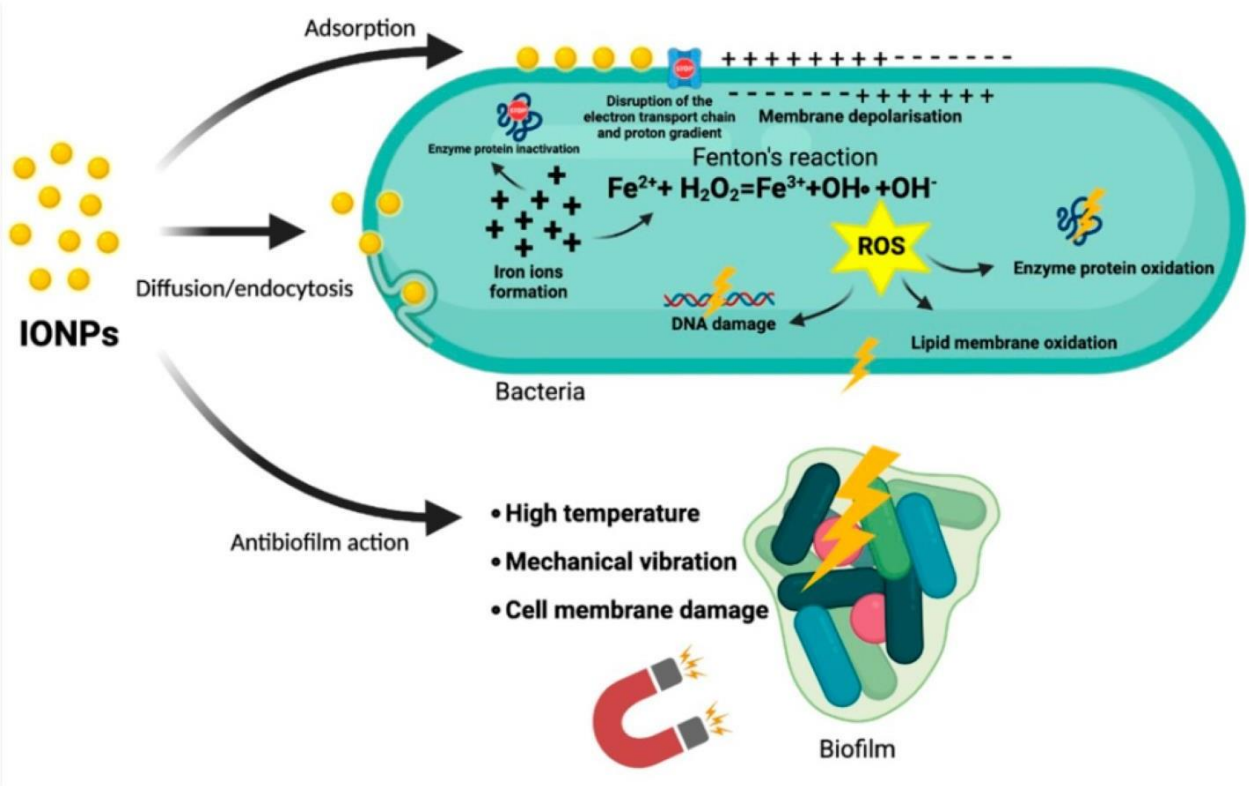

Figure 3: The mechanisms of IONP antibacterial activity (Arakha et al., 2015)

CHAPTER THREE

3. MATERIALS AND METHODES

3.1 Materials and Apparatus

The instruments and apparatus used include: XRD, UV/Visible spectrophotometer, reactor tube, analytical balance, pH meter, hot plate, furnace, ceramic crucible, agate mortar, centrifuge, water bath, thermometer, volumetric flasks, pipettes, graduated cylinders, desiccators, magnetic stirrer, test tubes, and beakers.

3.2 Chemicals and Reagents

The chemicals and reagents used in this work were ferric chloride hexa-hydrate ($FeCl_3.6H_2O$, Blulux Ltd, India), ferrous chloride tetra hydrate ($FeCl_2.4H_2O$, Atico, India), sodium hydroxide NaOH (Sigma Aldrich 99% purity), ethanol (C_2H_5OH, 99.9%) HCl (Riedel dehaen, Germany,37%),$FeSO_4.7H_2O$ (Sigma Aldrich 99% purity) *Calpurnia aurea* leaf.

3.3 Site of plant sample collection

"Cekata or Digita" (*Calpurnia aurea*), belongs to the family of *Fabaceae*, was collected from Arsi zone, Oromia region at Zuway dugda"a woreda in Arata Chufa kebele after conducting the field surveys. The leaves were thoroughly washed and rinsed with tape water followed by washing with distilled water to remove dust. Then the leaves were shade dried at room temperature for about 7 days in normal atmosphere. Dried leaves were cut into fine pieces, grinded to get the finest powder and weighed about 20g (Nurbaş. M et al., 2017).

3.4. Methods

3.4.1. Extraction of the leaves (broth solution)

A20g of powdered *Calpurnia aurea* leaves were boiled with 150 mL of distilled water at 30°C with stirring for about one hour until the solution turned light brown. The aqueous extract was then cooled and filtered, first using ordinary filter paper and then Whatman filter paper. The filtrate was stored in a refrigerator at 4°C for the synthesis of Fe_2O_3 and Fe_3O_4 nanoparticles, serving as a reducing agent.

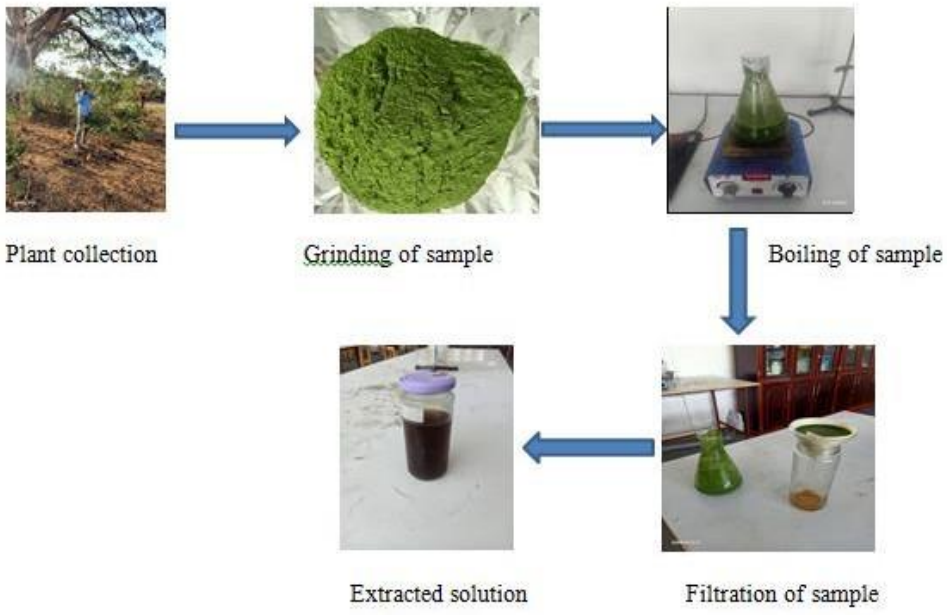

Figure 4: The preparation process of *culpurnia auria* leaf extract.

3.4.2. Synthesis of Fe_2O_3 Nano Particles using plant Extract

Calpurnia aurea leaves (20g) were used for extraction. First, 10g of $FeCl_3 \cdot 6H_2O$ was dissolved in 150ml of pure water while stirring at room temperature. Subsequently, the aqueous solution of Calpurnia aurea leaf extract was added to the mixture at a rate of 3 mL/min to achieve volume ratios of 1:1, 1:2, and 2:1, with continuous stirring at room temperature for 10 minutes using a magnetic stirrer. Following this, a 1.0 M NaOH solution was added until the pH reached 11. The resulting black dispersion was stirred continuously for 1 hour at room temperature, and then the Fe_2O_3 nanoparticles were harvested by evaporating the water from the solution. The obtained Fe_2O_3 nanoparticles were used to assess antibacterial activity.

Figure 5: Schematic diagram of synthesis process for Fe_2O_3 nanoparticles

3.4.3. Synthesis of Fe_3O_4 Nano Particles using plant Extract

Fe_3O_4 nanoparticles (NPs) were synthesized using a co-precipitation method with an aqueous leaf extract of *Calpurnia aurea* as a capping agent. In a typical procedure, $FeCl_3 \cdot 6H_2O$ and $FeSO4 \cdot 7H_2O$ were mixed in distilled water at a 2:1 molar ratio and stirred magnetically. The reaction mixture was then maintained at 100°C with constant stirring for 15 minutes under atmospheric conditions. After this, the aqueous solution of *Calpurnia aurea* leaf extract was added to the mixture at a rate of 3 mL/min to achieve volume ratios of 1:1, 1:2, and 2:1, while stirring at room temperature for 10 minutes using a magnetic stirrer. An 8M NaOH solution was then added drop wise to the reaction mixture at a rate of 3 mL/min until the pH reached 11, facilitating the precipitation of Fe_3O_4 nanoparticles. The resulting black precipitate of Fe_3O_4 NPs was filtered using Whatman No. 1 filter paper, washed with distilled water two to three times, and dried in an oven at 80°C for one hour for further use. The possible reaction is shown below.

$2FeCl_3.6H_2O(aq) + FeSO_4.7H_2O(aq) + NaOH + C.Aurea \rightarrow Fe_3O_4\downarrow + 6NaCl(aq) + Na_2SO_4 .17H_2O\ (aq)$

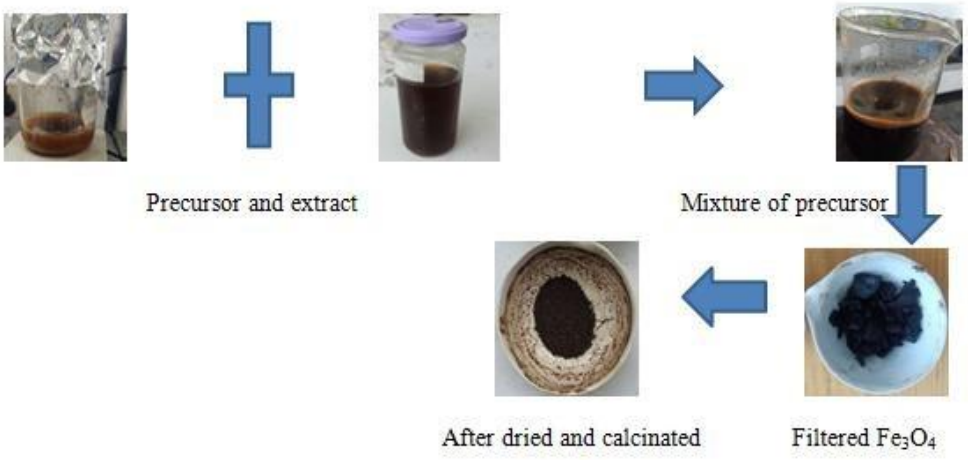

Figure 6: Schematic diagram of synthesized process for Fe_3O_4 nanoparticles

3.5 Common characterization Techniques for Fe_2O_3 and Fe_3O_4 nanoparticles

3.5.1 Characterization of Fe_2O_3 and Fe_3O_4 Nanoparticles Using XRD

To analyze structure of the newly synthesizing Fe_2O_3 and Fe_3O_4 Nps XRD was employed. The XRD patterns of Fe_2O_3 and Fe_3O_4 Nps was recorded on X-ray diffractometer at the range of 2θ from 10 to 80 with a scan rate of 20/ min using Cu Kα (λ = 1.5406 A^0) radiation with an accelerating voltage of 40 KV. Different phases present in the samples was evaluated (Saqib *et al.*, 2018). The average particle size was calculated with Debye Scherrer's formula.

$$D = {}^{0.9\lambda}/_{\beta cos\theta}$$

Where, D the Crystallite size, λ = 1.54 A_0 is the X – ray source wavelength, β is the Full Width at Half Maximum (FWHM) of a peak, and θ is the peak position ((Arokiyaraj et al., 2013)

3.5.2. Characterization of Fe_2O_3 and Fe_3O_4 Nanoparticles Using FTIR

The prepared Fe_2O_3 and Fe_3O_4 nanoparticle was subjected to FT-IR spectroscopy measurements. It was recorded by using spectrometer in the range 400 - 4000 cm^{-1} at a resolution of 4 cm^{-1} based on KBr pellet technique. It was used to identify the possible biomolecules responsible for the reduction and capping of the nanoparticles (Kumar and Ananthu, 2018).

3.5.3. Characterization of Fe_2O_3 and Fe_3O_4 Nanoparticles Using UV-Vis Spectoscopy

The surface plasmon resonances (SPR) of synthesized iron oxide nanoparticles have been studied by UV-Vis Spectrophotometer. The absorption of visible radiations due to the excitation of SPR,

imparts various colours to nanoparticles. As the nanoparticles size changes, colour of the solution also changes. So UV-Vis absorption spectrum is quite sensitive to the formation of nanoparticles. The UV-Vis absorption spectra of the Fe_2O_3 and Fe_3O_4 nanoparticles from *Calpurnia aurea* leaf extract and that of chemically synthesized was confirmed by using wave length scan between 200 nm and 800 nm (Bhosale *et al*. 2014). From the UV-Vis graphs, energy band gap was obtained using the formula:

$$Eg = 1240 / \lambda max \ eV = hc \ \cdots\cdots\cdots\cdots (2)$$

Where Eg is energy band gap, h is planks constant, c is speed of light and λ is the maximum wavelength of the synthesized Fe_2O_3 and Fe_3O_4 nanoparticles.

3.5.4. Characterization of Fe_2O_3 and Fe_3O_4 Nanoparticles Using SEM

The scanning electron microscopy was carried out to study the surface morphology of Fe_2O_3 and Fe_3O_4 NPs. The nanoparticles was taken and mounted with double adhesive tape on stubs, sputtercoated with gold palladium. To analyze morphological features of Fe_2O_3 and Fe_3O_4 NPs field emission scanning electron microscope was used at an accelerating voltage of 10 KV upon gold coating for 4 min. The chemical compositions of the biosynthesized Fe_2O_3 and Fe_3O_4 NPs nanoparticles was estimated by energy-dispersive X-ray spectroscopy Energy dispersive X-ray analysis attached with SEM determined presence of different elements in the NPs sample. The specimen was determined through energy-dispersive X-ray spectroscopy software that applies ZAF correction and carries out subsequent integration of the peaks to get the final quantification of the elements present in the sample (Saqib.S et al., 2018).

3.6. Method for Antibacterial Activity

Materials used for anti-bacterial activity of Fe_2O_3 and Fe_3O_4 NPs are 0.2g nutrient broth, Erlenmeyer flask, Cotton, autoclave, Petri plates, Fe_2O_3 and Fe_3O_4 NPs, 2g agar, *Staphylococcus aureus*, *Streptococcus pyogenes*, *Pseudomonas aeruginosa and Escherichia coli*. Disc diffusion method was used for antibacterial activity of iron oxide (Fe_2O_3 and Fe_3O_4) nanoparticles.

3.6.1. Preparation of Inoculum

0.2g nutrient broth was dissolved in 25 mL distilled water prepared in two Erlenmeyer flasks. Cotton plugs the flask and sterilized it in autoclave at 121 ^{0}C for 15 min. In one conical flask clinically isolated strain of *Staphylococcus aureus* and *Streptococcus pyogenes*, was inoculated. In the other conical flask clinically isolated strain of *Escherichia coli* and *Pseudomonas aeruginosa* was added. Inoculums of all the strains were developed in this growth media. A loop full of bacterial strain was added in it and it was left over night at 37^{o}C in shaking incubator. This was diluted up to 10^{-2} before inoculating the plates (Gupta and Gupta, 2005).

3.6.2. Disc diffusion Method for Antibacterial Activity

2g agar and 0.8g nutrient broth were mixed to make 100 mL solution in an Erlenmeyer flask. Cotton plugs the flask and sterilized it. Poured about 15 to 20 ml of agar in Petri plate, solidified it and then inoculate it with the bacterial strain. Wells having diameter of 0.4 cm will be developed in which 10 μL of sample suspension was added. Suspensions of all samples were prepared by dissolving 25 mg, 50 mg and 75 mg of product in1 mL DMSO. These plates will be kept for 24 hours at 37 ^{0}C and zones of inhibition were observed (Gupta and Gupta, 2005).

CHAPTER FOUR

4. Results and Discussion

4.1 Observed results during the biosynthesis of (Fe_2O_3) and (Fe_3O_4) NPs

This section mainly compared the result of green synthesized method of iron oxide hematite (Fe_2O_3) and magnetite (Fe_3O_4) nanoparticles by using different precusory depending on their method of synthesized. The green method iron oxide (Fe_2O_3) and (Fe_3O_4) nanoparticles synthesized in different ratios from ferrous sulphate hepta hydrate and ferric chloride hexa hydrate as precursors and leafs of *Calpurnia aurea* extract as a reducing and capping agent. Also the different characterization methods of green synthesized iron oxide (Fe_2O_3) and (Fe_3O_4)comparing nanoparticles and its application for anti-bacterial activity presented.

In the current study, Fe_3O_4-NPs synthesized by green method was carried out in presence of NaOH which yields 1:1,1:2,and 2:1 nanoparticle was 4.8 nm, 5.3 nm and 9.8 nm respectivelyand the Fe_2O_3-NPs was 11.3,11.5 and 11.9nm average size. Hence, the method of synthesis utilized here for obtaining Fe_2O_3-NPs and Fe_3O_4-NPs imparts uniformity in size and morphologyto them.

4.2. X-ray Diffraction (XRD) Analysis

4.2.1 XRD Analysis of Fe_2O_3 Nps

Evaluation of crystal structure in samples conducted using XRD obtained the conformity of XRD data with the peaks that appear in International Centre Diffraction Data (ICDD). The XRD patterns of the synthesized Fe_2O_3Nps are shown in Figure 7 (Hakim et al., 2023).

This observed finding is in agreement with the similar reported for iron oxide nanoparticles. As shown in figure 7, the diffraction peak of Fe_2O_3Nps were detected at 2θ (degree) = 24.1, 33.27, 35.69, 40.87, 49.44, 54.12, 57.68, 62.37, 63.99 for Fe_2O_3Nps at 2:1 ratio, 2θ (degree) = 24.21, 33.27, 35.69, 40.87, 49.44, 54.12, 57.68, 62.53, 63.99 for Fe_2O_3Nps at 2:1 and 2θ (degree) = 24.17, 33.20, 36.65, 40.99, 49.56, 54.25, 57.81, 62.5, 64.1 , which typically All the peaks of the sample located at the specified 2θ positions are consistent with the standard value of single phase α-Fe2O3, (ICDD No. 01-079-0007) (Shariatzadeh et al., 2022), (Lassoued.A et al., 2017) .

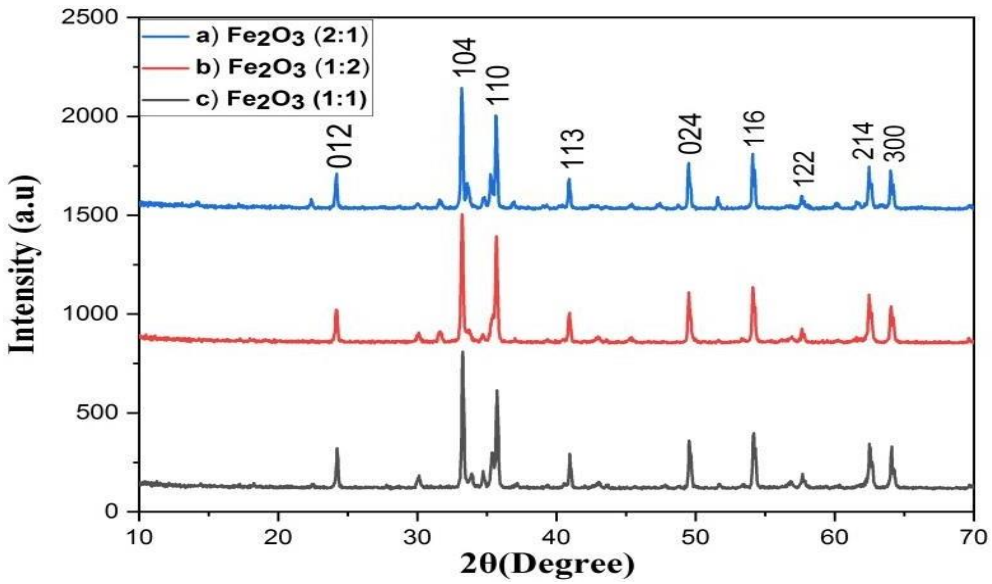

Figure 7: XRD Pattern of Fe_2O_3 NPs

These peaks were confirmed to be rhombohedral structures of hematite with space group R3c, representing the orientation planes (012), (104), (110), (113), (024), (116), (122), (214), (300), (119), and (220), respectively (Valladares D.L et al., 2019). The reflection of other diffraction peaks associated with the crystalline phase and other impurities were not detected in each of the samples with various calcinations, indicating that hematite (α-Fe2O3) synthesized in biogenic method in this study is a pure phase without significant impurities (Fardood S.T et al., 2017). The observed peak, corresponding to the (104) orientation plane in Figure 7, was the highest in the XRD diffraction pattern, indicating it is the intensity peak.

Crystallite size generally corresponds to the coherent volume in the material for the respective diffraction peak. Sometimes, it also corresponds to the size of the grains of a powder sample, or thickness of polycrystalline thin film or bulk material. The Scherrer's equation

$$D = K\lambda / \beta cos\theta \quad \ldots\ldots\ldots\ldots\ldots\ldots\ldots\ldots\ldots\ldots (3)$$

Where D is the crystallite size (nm), *K represents the Scherrer constant (0.98), λ is the X-ray wavelength of Cu Kα= 0.154 nm* and β is the peak width of half-maximum) is used for determination of size of particles of crystals in the form of powder (Rufus.A, 2017).

It was found that the value of the crystallite size of the hematite nanoparticles was 11.98 nm for Fe_2O_3Nps at 2:1, 11.59 nm for Fe_2O_3 at 1:2 and 11.39 nm for Fe_2O_3Nps at 1:1 ratios respectively. The difference in the sizes of the particles can be due to the difference in concentration between Fe_2O_3Nps.

As shown in table 1The calculated lattice parameters of the synthesized hematite nanoparticles (NPs) and *Calpurnia aurea*

Table 1: Interplanar spaces (d-hkl), FWHM values, lattice parameter, and crystallite sizes of Fe_2O_3Nps.

Fe_2O_3-(2-1)										
2θ Value (deg)	θ Value (deg)	θ Value (rad)	dhkl(A)	FWHM(deg)	FWHM(rad)	hkl	(h^2+ k^	SQRT(h^2 + k^2+l^2)	Lattice parameter(α) in Å	Crystallite size (nm)
24.1657	12.0828	0.21089	3.68278	0.69041	0.01205	12	5	2.23607	8.23494	11.7765
33.2481	16.6241	0.29014	2.6946	0.76652	0.01338	104	17	4.12311	11.1101	10.8246
35.5952	17.7976	0.31063	2.52212	0.81531	0.01423	110	2	1.41421	3.56682	10.2416
40.9034	20.4517	0.35695	2.20624	0.70045	0.01223	113	11	3.31662	7.31727	12.1141
49.545	24.7725	0.43236	1.83978	0.69756	0.01217	24	20	4.47214	8.22776	12.5527
54.1562	27.0781	0.4726	1.69352	0.70187	0.01225	116	38	6.16441	10.4396	12.7221
57.6948	28.8474	0.50348	1.59779	0.71499	0.01248	122	10	3.16228	5.05266	12.6951
62.5248	31.2624	0.54563	1.48548	0.79949	0.01395	214	21	4.58258	6.8073	11.6336
64.0848	32.0424	0.55925	1.45303	0.70282	0.01227	300	9	3	4.35909	13.3453
								Average Size		11.9895
Fe_2O_3-(1-2)										
2θ Value (deg)	θ Value (deg)	θ Value (rad)	dhkl(A)	FWHM(deg)	FWHM(rad)	hkl	(h^2+ k^	SQRT(h^2 + k^2+l^2)	Lattice parameter(α) in Å	Crystallite size (nm)
24.1857	12.0929	0.21106	3.67977	0.69771	0.01218	12	5	2.23607	8.22822	11.6537
33.2623	16.6311	0.29027	2.69349	0.75655	0.0132	104	17	4.12311	11.1055	10.9677
35.6101	17.805	0.31076	2.5211	0.77029	0.01344	110	2	1.41421	3.56538	10.8406
40.9038	20.4519	0.35695	2.20622	0.69933	0.01221	113	11	3.31662	7.31721	12.1335
49.5713	24.7856	0.43259	1.83887	0.70374	0.01228	24	20	4.47214	8.22369	12.4437
54.1567	27.0784	0.47261	1.69351	0.72878	0.01272	116	38	6.16441	10.4395	12.2523
57.4068	28.7034	0.50097	1.60512	1.17715	0.02055	122	10	3.16228	5.07583	7.70023
62.5002	31.2501	0.54542	1.486	0.74334	0.01297	214	21	4.58258	6.80971	12.5108
64.1082	32.0541	0.55945	1.45256	0.67816	0.01184	300	9	3	4.35767	13.8324
								Average Size		11.5928
Fe_2O_3-(1-1)										
2θ Value (deg)	θ Value (deg)	θ Value (rad)	dhkl(A)	FWHM(deg)	FWHM(rad)	hkl	(h^2+ k^	SQRT(h^2 + k^2+l^2)	Lattice parameter(α) in Å	Crystallite size (nm)
24.2349	12.1175	0.21149	3.67241	0.69279	0.01209	12	5	2.23607	8.21176	11.7375
33.313	16.6565	0.29071	2.6895	0.76899	0.01342	104	17	4.12311	11.0891	10.7917
35.6166	17.8083	0.31081	2.52065	0.81096	0.01415	110	2	1.41421	3.56474	10.2972
40.9347	20.4674	0.35722	2.20463	0.69988	0.01222	113	11	3.31662	7.31192	12.1252
49.6051	24.8025	0.43289	1.8377	0.70427	0.01229	24	20	4.47214	8.21844	12.4361
54.2076	27.1038	0.47305	1.69204	0.73175	0.01277	116	38	6.16441	10.4304	12.2054
57.4325	28.7163	0.50119	1.60446	1.32835	0.02318	122	10	3.16228	5.07376	6.82458
62.5248	31.2624	0.54563	1.48548	0.744	0.01299	214	21	4.58258	6.80731	12.5013
64.1382	32.0691	0.55971	1.45195	0.68728	0.012	300	9	3	4.35584	13.6511
								Average Size		11.3967

4.2.3 X-ray diffraction analysis of biosynthesized Fe_3O_4 NPs

Figure 8 (a, b and c) shows the XRD patterns of Fe_3O_4 NPs synthesized from ferric chloride hexa-hydrate ($FeCl_3.6H_2O$), ferrous chloride tetra hydrate ($FeCl_2.4H_2O$) as precursor and *Calpurnia aurea* Leaf Extract leaf extract. Fe_3O_4 NPs were synthesized in three ratios by volume of iron salt precursors to *Calpurnia aurea* leaf extract. These ratios by volume were taken Fe_3O_4 NPs for 2:1, 1:1 and for 1:2 ratios of precursors to plant extract.

The results of peak position (θ), Full Width at Half Maximum (FWHM) of a peak, d-spacing (dhkl) and Miller indices (hkl) for Fe_3O_4nanoparticles were calculated using an Interactive Powder Diffraction Data Interpretation and indexing program software from XRD data.

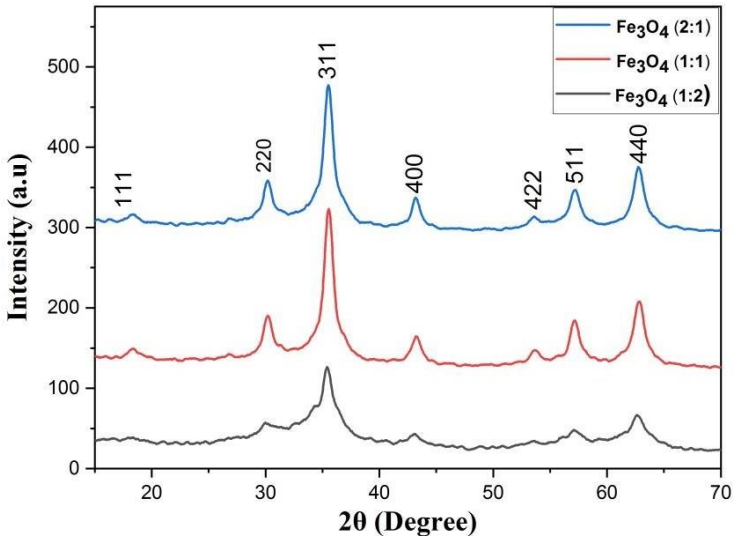

Figure 8: XRD Pattern of Fe_3O_4 NPs

As shown in figure 8, the diffraction peak of Fe_3O_4 nanoparticles were detected at 2θ (degree) = 18.24, 30.25, 35.48, 43.17, 53.57, 57.23, 62.7 for Fe_3O_4 NPs at 2:1 ratio, 2θ (degree) = 18.34, 30.24, 35.53, 43.17, 53.62, 57.13, 62.81 for Fe_3O_4 NPs at 1:1 ratio and , 2θ (degree) = 30.24, 35.36, 43.08, 53.7, 57.03, 62.71 for Fe3O4 NPs at 1:2 ratio (Kiwumulo H.F et al., 2022).

The X-ray diffraction patterns all of the samples at 2θ (degree) correspond with hkl plane in a crystal lattice i.e., (2 2 0), (3 1 1), (4 0 0), (422), (5 1 1), and (4 4 0) (Pandey et al., 2023). The well-developed peaks at certain angle with sharp peak intensity indicate that samples are highly crystalline in nature.

Table 2: Interplanar spaces (d-hkl), FWHM values, lattice parameter, and crystallite sizesof Fe_3O_4 NPs.

Fe_3O_4-(1:1)										
2θ Value (deg)	θ Value (deg)	θ Value (rad)	dhkl(A)	FWHM(deg)	FWHM(rad)	hkl	(h^2+ k^	SQRT(h^2 + k^2+l^2)	Lattice parameter(α) in Å	Crystallite size (nm)
30.11762	15.05881	0.262826	2.967164	9.10274	0.158873	220	8	2.828427	8.392408	0.90448
35.45522	17.72761	0.309405	2.531757	1.61542	0.028194	311	11	3.316625	8.396888	5.16697
43.08611	21.54306	0.375997	2.099399	1.3452	0.023478	400	16	4	8.397597	6.35414
57.34106	28.67053	0.500395	1.606804	3.48272	0.060785	511	27	5.196152	8.349198	2.60184
62.81954	31.40977	0.548204	1.479214	2.32441	0.040569	440	32	5.656854	8.367698	4.00771
									Average Size	3.80703
Fe_3O_4-(2:1)										
2θ Value (deg)	θ Value (deg)	θ Value (rad)	dhkl(A)	FWHM(deg)	FWHM(rad)	hkl	(h^2+ k^	SQRT(h^2 + k^2+l^2)	Lattice parameter(α) in Å	Crystallite size (nm)
18.32872	9.16436	0.159948	4.840296	0.36625	0.006392	111	3	1.732051	8.383638	21.9885
30.24325	15.12163	0.263922	2.955124	1.27714	0.02229	220	8	2.828427	8.358354	6.4485
35.54904	17.77452	0.310224	2.52529	1.24208	0.021678	311	11	3.316625	8.37544	6.7218
43.24793	21.62397	0.377409	2.091918	0.89526	0.015625	400	16	4	8.367674	9.55295
53.71958	26.85979	0.468792	1.706253	0.90396	0.015777	422	24	4.898979	8.358898	9.85878
57.18038	28.59019	0.498993	1.610936	1.21028	0.021123	511	27	5.196152	8.370671	7.48136
62.80624	31.40312	0.548088	1.479495	1.42187	0.024816	440	32	5.656854	8.369289	6.55116
									Average Size	9.80043
Fe_3O_4-(1:2)										
2θ Value (deg)	θ Value (deg)	θ Value (rad)	dhkl(A)	FWHM(deg)	FWHM(rad)	hkl	(h^2+ k^	SQRT(h^2 + k^2+l^2)	Lattice parameter(α) in Å	Crystallite size (nm)
30.62382	15.31191	0.267243	2.919263	4.10812	0.0717	220	8	2.828427	8.256921	2.00653
35.52996	17.76498	0.310057	2.526602	1.65512	0.028887	311	11	3.316625	8.379792	5.04409
43.20683	21.60342	0.377051	2.093813	1.12147	0.019573	400	16	4	8.375252	7.62495
57.16987	28.58494	0.498901	1.611208	1.50705	0.026303	511	27	5.196152	8.37208	6.00782
62.78638	31.39319	0.547915	1.479915	1.49281	0.026054	440	32	5.656854	8.371665	6.23918
									Average Size	5.38452

Diffraction peaks shown by synthesized samples are consistent with the standard pattern of magnetite nanoparticles (JCPDS Card No. 79 - 0417). All synthesized samples show very broad peaks, indicating the ultra-fine nature of the particles (Upadhyay et al, 2016).

The average crystalline size calculated using Debye-Scherer equation of the diffraction peaks of Fe_3O_4 NPs for these three ratios by volume were found to be 9.80 nm, 5.38 nm and 4,82 nm for Fe_3O_4 Nps at 2:1, Fe_3O_4 Nps 1:2, and Fe_3O_4 Nps 1:1 ratio, respectively. Even though the three F_3O_4 NPs of different proportions were prepared by the same procedure, there is a slight shift of 2θ position for certain peaks.

This might be due to the different ratios of precursors and extracts used that might result in nanoparticles with different sizes, shapes and morphologies. The decreasing in intensity or shifting the peak suggested that interaction of biomolecules present in both precursor and plant leaf extract (Urvashi Kheskwani and M. Mansoor Ahammed, 2023).

4.3 FTIR Analysis of Fe_2O_3 Nps and Fe_3O_4 Nps

FTIR is a very versatile tool for surface characterization of nanoparticles Under specific conditions, the NPs surface chemical composition can be determined, and additionally, the reactive surface sites responsible for the surface reactivity can be identified. FTIR spectroscopy is a technique used to identify the characteristic functional groups from the spectral bands that allow us to know the conjugation between the nanomaterial and the adsorbed biomolecules (Rivero K.T et al., 2021).

The infrared spectra presented in this work were recorded in the range from 400 to 4000 cm^{-1} with FT-IR spectrometer. Fourier transform infra-red (FTIR) spectra of Fe_2O_3 and Fe_3O_4Nps were shown in Figure 9. Measurements of were performed by putting the powder of Fe_3O_4 NPs on KBr plate.

The FTIR spectrum of green synthesized Fe_2O_3 nanoparticles showed peaks at 1973.13, 1453.47, 539.67, 522.64, 481.92, 448.11, and 433.11, cm^{-1}. The FTIR spectrum at 1973.13 cm^{-1} corresponds to the presence of C-H stretching indicating the existence of small amount of aromatics functional group adsorbed to the NPs (Ndou.N et al., 2023).

The peak at 1425 cm^{-1} was attributed to the stretching vibrations of the -CH_2 bending functional group (Geneti S.T et al., 2022). The high frequency band at 539-522 cm^{-1} can be attributed to Fe-O deformation in the octahedral and tetrahedral regions, while the low frequency band at 448 – 433,37 cm^{-1} can be related to the Fe-O deformation in the octahedral region of hematite (Bonzkurt.G, 2020).

The FTIR spectra of synthesized Fe_3O_4 Nps samples were shown in figure 9.The FTIR spectrum of green synthesized iron oxide magnetite nanoparticles showed peaks at 3280, 2918.07, 2850, 1730.40, 1601.54, 1412.59, 1024.93, and 512.25 cm^{-1}. The FTIR spectrum at 3280 cm^{-1} corresponds to the presence of O-H stretching indicating the existence of small amount of water adsorbed to the NPs (Mohamed.M et al., 2023). The weak peak situated at aproximately 2918-2850 cm^{-1} could be attributed to symmetric C–H vibrations (Dwivedi.P et al., 2024).

the absorption band around 1730 $cm^{-1}$and 1601.54 cm^{-1} corresponds to asymmetric stretching of C=O bonds from the COOH group (Nalbandian.L et al., 2015). The peak around 1412 $cm^{-1}$and 1024.93 cm^{-1}could is due to bending vibration of C-N stretch and C-O stretching of bonds (Taib N.I et al., 2018). The peak appearing at around 512 cm^{-1} was assigned to the metaloxygen (Fe–O) stretching modes (Nurbaş. M et al., 2017).

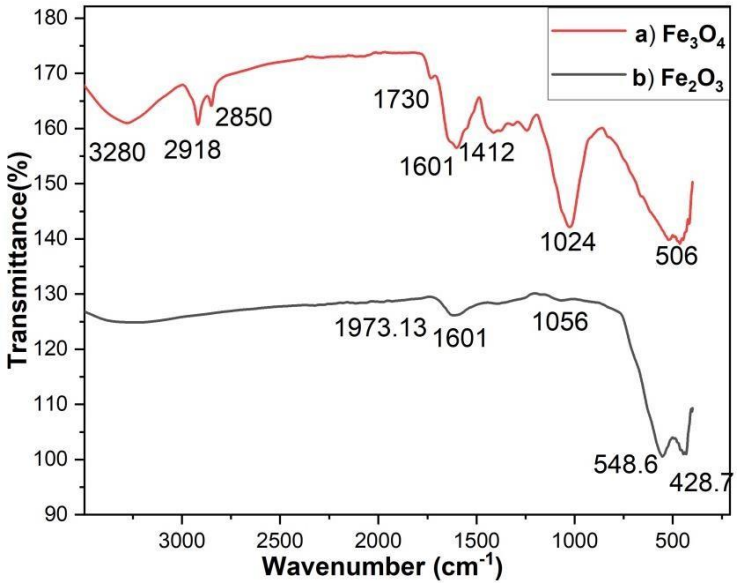

Figure 9: FTIR spectra of Biosynthesized (a) Fe_3O_4 Nps (b) Fe_2O_3 Nps

4.4 UV-Vis DRS analysis of biosynthesized Fe_2O_3 and Fe_3O_4 Nps

UV-Vis diffuse reflectance spectroscopy is useful for identifying diverse types of iron oxides and to obtain information about the optical properties. It can be clearly seen from figure10 that absorbance of Fe_2O_3 is in the range of 200–850 nm indicating that the band edge absorption has been broadened to visible light region (Parhizkar.J, Habibi M.H, 2017). The spectra in show a nearly constant decline in reflectivity in the range 350 nm from invisible region to 560 nm around yellow region, started from 560 nm; reflectivity becomes constant near 800 nm up to red region (Valášková.M et al., 2019).

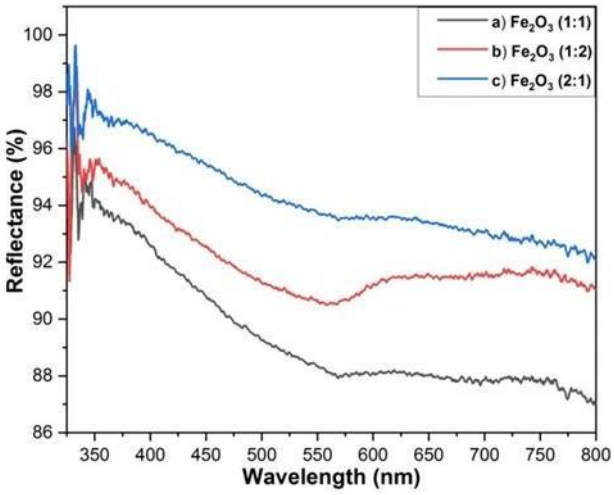

Figure 10: Reflectance (%) of Biosynthesized Fe_2O_3Nps at different ratio

The Kubelka-Munk equation was used to plot $(F(R)h\nu)^{1/2}$ versus E and determine the energy band gap of the samples. Figure 11 exhibits the graphical representation of the Kubelka-Munk method and the respective band gaps of all compositions (Araujo.R et al., 2021). The Fe_2O_3 Nps composition presents a band gap of which is related to other values reported in the literature for hematite. The synthesized Fe_2O_3 Nps at 1:1, 1:2, and 2:1 ratios presented band gap values of 1.85, 1.89, and 1.91 eV, respectively, slightly lower than that of pure iron oxide composition which is 2.1 eV (Xu Zong, Can Li, 355-399). The lower band gaps might have resulted from due to decrease in the precursor concentration.

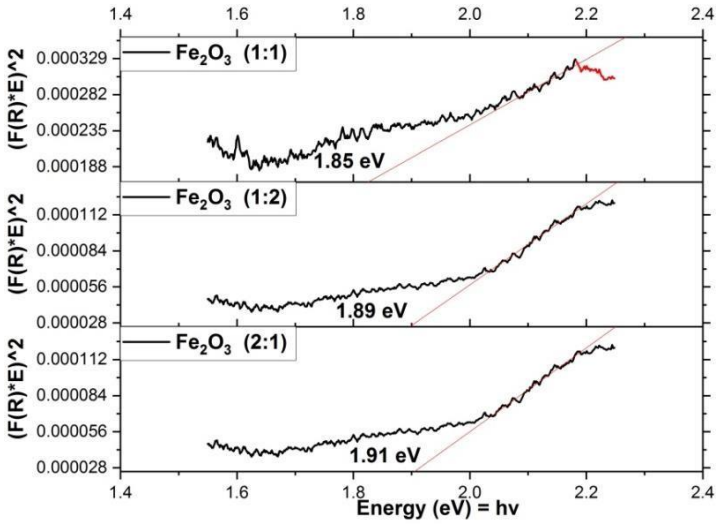

Figure 11: Tauc plot for Biosynthesized Fe_2O_3 at different ratio

UV-Vis DRS reflectance spectra of both synthesized Fe_3O_4 Nps were shown in Figure 9. The diffuse reflectance spectrum of sample Fe_3O_4 NPs indicates that a sharp increase of the reflectance in the range of 400-750 nm, typical for Fe_3O_4 Nps nano powders with a black color which is related to the literature value (Anamika et al., 2020).

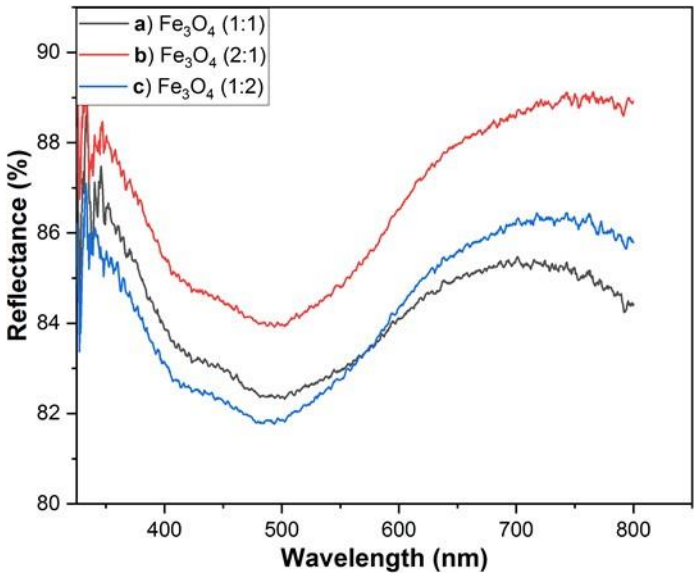

Figure 12: Reflectance (%) of Biosynthesized Fe_3O_4 NPs at different ratio

As shown from the figure 9 Fe_3O_4 Nps synthesized at 2:1 ratio had the greatest band gap energy (1.85 ev) than Fe_3O_4 Nps synthesized at 1:1 and Fe_3O_4 Nps synthesized at 1:2 ratio (1.80 ev and 1.41 ev).This is due to the magnetite surface is covered with relatively low amount of coating material (*C.Aurea*) which might be increase the incident light reflection by the sample. As shown from the graph Fe_3O_4 Nps at 1:1 ratio and 1:2 ratio the presence of extra concentration of *C.Aurea* decreases, the refelectance intensity of synthesized Fe_3O_4 Nps.

4.5 SEM analysis of biosynthesized Fe_2O_3 and Fe_3O_4 Nps

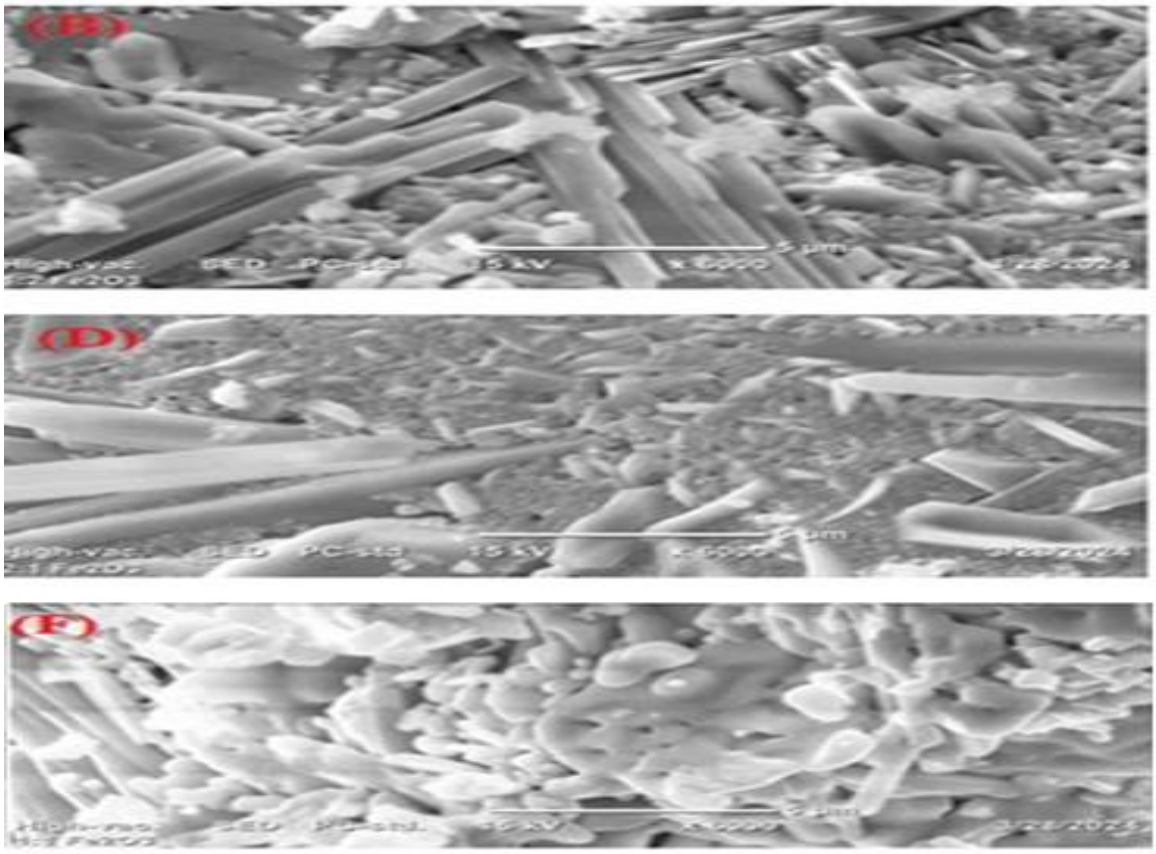

Figure 13: SEM Analysis of Biosynthesized Fe_2O_3 Nps

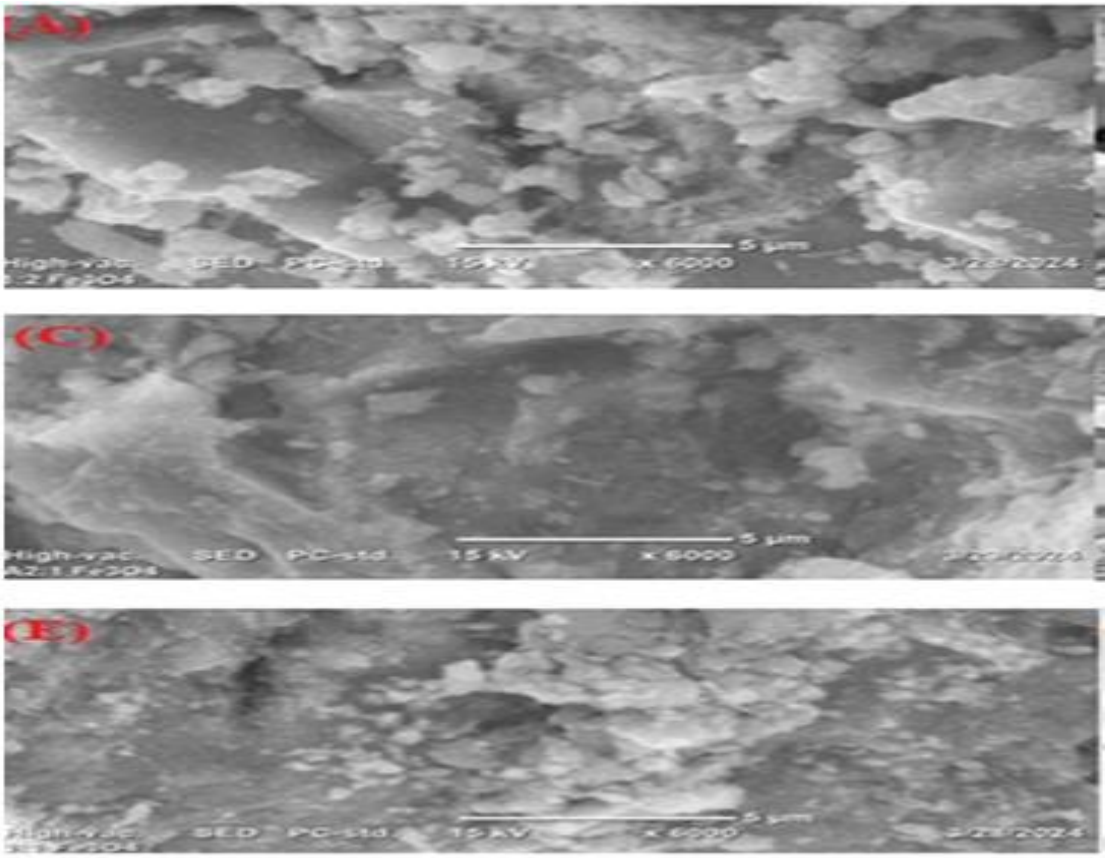

Figure 14: SEM Analysis of Biosynthesized Fe_3O_4 Nps

Analysis by SEM was carried out to study the morphologies of hematite and magnetite samples obtained using scanning electron microscopy are shown in figures (A–F). The magnetite samples 1:2 Fe_3O_4 (A), 2:1 Fe_3O_4 (C), and 1:1 Fe_3O_4 (E) are irregular, bulkier, and aggregated. Fe_3O_4 morphology was studied using SEM providing insights into the crystalline phase formation. Additionally, SEM analysis was conducted on Fe_3O_4 nanoparticles for 4000X magnification, showing the surface morphology of the nanoparticles

The rods are formed of hematite 1:2 Fe_2O_3 (B), 2:1 Fe_2O_3 (D), and 1:1 Fe_2O_3 (F). Increasing the firing temperature reduces carbon and oxygen, making the particles rod-like. In a study by (Sahoo et al., 2011), the characterization of Fe_2O_3 nano powders synthesized by an emulsion precipitation-calcination route was conducted. Additionally, the rheological behavior of Fe_2O_3 was investigated. This research provides insights into the synthesis and characterization of iron oxide nano powders. Furthermore, (Mishra et al., 2008) utilized scanning electron microscope (SEM) images to model the mineral dust optics of the Indian Desert. The study focused on realistic dust shapes, including spheres, spheroid, Chebyshev, and cylinders, to analyze the

optical properties of mineral dust. Overall, the studies provide valuable information on the characterization, synthesis, and optical properties of hematite and magnetite nanoparticles, shedding light on these nanoparticles' shape and size analysis under a scanning electron microscope.

4.6 Antibacterial Activity of Fe_2O_3 and Fe_3O_4 Nps

Clinical bacterial strains with American Type Culture Collection (ATCC) including *E. coli* (ATCC 25922), *P. aeruginosa* (ATCC-27853), *S. pyogenes* (*ATCC-19615*) and *Staphylococcus aureus* (ATCC 25923) were used to evaluate the antibacterial activity of the 1:1 Fe_2O_3, 1:2 Fe_2O_3, 2:1 Fe_2O_3, 1:1 Fe_3O_4, 1:2 Fe_3O_4 and 2:1 Fe_3O_4 nano particles synthesis. The standard bacterial cultures were obtained from Ethiopian Biodiversity Institute, Addis Ababa, Ethiopia. McFarland 0.5 standard was prepared by mixing 99.95 mL 1% H_2SO_4 in distilled water and 0.05 mL 1% $BaCl_2$ in distilled water to estimate bacterial density using UV-Vis spectrophotometer at 600nm wavelength with absorbance of 0.11. The antibacterial susceptibility for the above synthesized NPs was evaluated by the agar disk diffusion method (Bauer et al., 1966) and prepared in DMSO to give 300, 150, 75, 37.5, and 18.75 mg/ml. Bacteria cell suspensions were adjusted to meet 0.5 McFarland turbidity standards to prepare 1.5×10^8

CFU/mL inoculum. Each bacterial suspension was inoculated on Mueller-Hinton agar plates using sterilized cotton swab, and the plates were allowed to dry for 5 min. The sterile filter paper disks were soaked in 300, 150, 75, 37.5, and 18.75 mg/ml of each concentration of synthesized NPs. The soaked filter paper disks were placed on the Mueller-Hinton agar plates and incubated at 37°C for 24hrs. The analysis was conducted in triplicate. Ceftriaxone 30 µg/mL disk was used as the positive control. After incubation, the zones of inhibition were recorded as the diameter of the growth free zones measured in mm using digital antibiotic zone reader.

In this study, the bacterial activity of magnetite (1:1 Fe_30_4, 1:2 Fe_30_4, 2:1 Fe_30_4) and hematite (1:1 Fe_20_3, 1:2 Fe_20_3, 2:1 Fe_20_3) was investigated using agar disc diffusion method against four bacterial strains (two Gram negative: *Escherichia coli* and *Pseudomonas aeruginosa* and two Gram positive: *Staphylococcus aureus* and *Streptococcus pyogenes*). The table 3 below shows the antibacterial activity of magnetite and hematite Nano particles against four pathogenic bacteria species. The activity of different ratios of magnetite and hematite showed varying degrees of inhibitory activity against *E. coli*, *P. aeruginosa*, *S. aureus and S. pyogenes* at

different concentrations. The synthesized iron oxide nano particles have moderate antibacterial activity against gram positive and gram-negative bacteria. In this study, magnetite nanoparticles were found to be a better antibacterial activity compared to hematite nanoparticles. Among the magnetite nanoparticles ratios 1:1 Fe_3O_4 exhibited the highest inhibition zone against *P. aeruginosa* (10.34±0.47mm) at the concentration of 300mg/ml. The lowest zone of inhibition against *E. coli and P.aeruginosa* was observed at a concentration of 18.75 mg/ml (6.34 ± 0.47 mm) with mean and standard deviation respectively. In contrast, the highest zone of inhibition against *S. aureus* was observed with hematite 1:1 Fe_2O_3 at a concentration of 300 mg/ml (10.33 ± 0.47 mm) and the lowest at theconcentration of 18.75mg/ml (6.33±0.47mm) for the *S. pyogens*.

Chemical composition can affect their ability to interact with bacterial cells and inhibit antibacterial effects. Impact The small crystalline structure of magnetite can interact with bacterial cells and disrupt cellular processes involved in bacterial growth and survival. Hence, the zone of inhibition of magnetite Fe_3O_4 is larger in this study. Magnetite and hematite nanoparticles can exhibit redox activity, which is important for the formation of reactive oxygen species that induce oxidative stress in bacterial cells and cause damage to bacterial cellular components.

Synthesized magnetite and hematite nanoparticles, incorporating C. aurea for antibacterial activity, were applied to polyester fabric, creating multifunctional fabric with magnetic, antibacterial, and sono-Fenton catalytic properties. The study showed enhanced tensile strength and excellent antibacterial activity against Staphylococcus aureus. (Gabrielyan et al., 2021) Confirmed moderate antimicrobial activity of magnetite nanoparticles. These findings highlight the potential of iron oxide nanoparticles, particularly magnetite and hematite, for various biomedical and environmental applications due to their significant antibacterial properties.

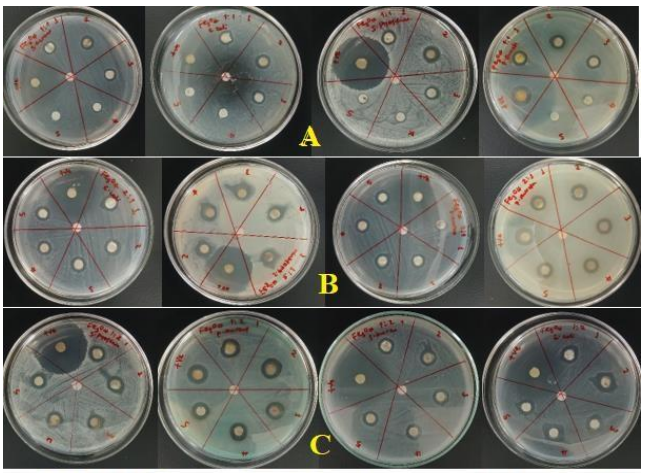

A) 1:1 Fe_3O_4 **B)** 2:1 Fe_3O_4 **C)** 1:2 Fe_3O_4

Figure 15: Antibacterial Activity of Fe_2O_3 Nps

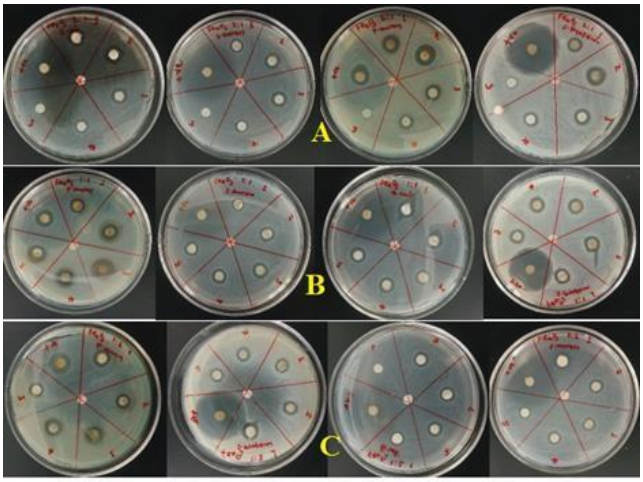

A) 2:1 Fe_2O_3 **B)** 1:1 Fe_2O_3 **C)** 1:2 Fe_2O_3

Figure 16: Antibacterial Activity of Fe_3O_4Nps

CHAPTER FIVE

5. Conclusion and Recommendations

5.1. Conclusion

In this study, the bacterial activity of magnetite Nps (1:1 Fe_30_4, 1:2 Fe_30_4, 2:1 Fe_30_4) and hematite Nps (1:1 Fe_20_3, 1:2 Fe_20_3, 2:1 Fe_20_3) comparing was investigated using agar disc diffusion method against four bacterial strains (two Gram negative: *Escherichia coli* and *Pseudomonas aeruginosa* and two Gram positive: *Staphylococcus aureus* and *Streptococcus pyogenes*). using *C.Aurea* leaf extract *Culpuria.Aurea* leaf extracts with high polyphenols content act as both reducing and capping agents for the nanoparticles. Furthermore, by changing the amount of the precursor material, the shape and size of the nanoparticles can be controlled which possesses benefits for synthesis process. The formation, structure, size, and surface morphology of the synthesized Fe_2O_3 and Fe_3O_4 Nps have been characterized by using different characterization techniques such as FTIR, XRD, SEM, DRS and UV-Vis analysis Among the magnetite nanoparticles ratios 1:1 Fe_3O_4 exhibited the highest inhibition zone against *P. aeruginosa* (10.34±0.47mm) at the concentration of 300mg/ml. The lowest zone of inhibition against *E. coli and P.aeruginosa* was observed at a concentration of 18.75 mg/ml (6.34 ± 0.47 mm) with mean and standard deviation respectively. In contrast, the highest zone of inhibition against *S. aureus* was observed with hematite 1:1 Fe_2O_3 at a concentration of 300 mg/ml (10.33 ± 0.47 mm) and the lowest at theconcentration of 18.75mg/ml (6.33±0.47mm) for the *S. pyogens*. Finally, magnetite nanoparticles were found to be a better antibacterial activity compared to hematite nanoparticles.

5.2 Recommendation

This study employed *Calpurnia aurea* leaf extract to green synthesize eco-friendly Fe_3O_4 and Fe_2O_3 nanoparticles, assessing their antibacterial efficacy against both gram-negative (*Escherichia coli, Pseudomonas aeruginosa*) and gram-positive bacteria (*Staphylococcus aureus, Streptococcus pyogenes*). Subsequent research should continue comparing these nanoparticles for similar applications to gauge their efficacy. *C. aurea* has a rich history in traditional medicine, treating ailments ranging from dysentery to cancer, showcasing diverse therapeutic properties. With the pressing global need for novel antimicrobial drugs, particularly in developing regions, further exploration of *C. aurea's* therapeutic potential is essential. Bacteria like Staphylococcus, Streptococcus, Pseudomonads, and Enterobacteriaceae pose significant challenges due to their resistance to existing antibiotics, necessitating innovative treatments. Promoting the utilization of herbal medicine demands rigorous evaluation and validation of traditional remedies. Despite their promising antibacterial qualities, magnetite and hematite nanoparticles require additional research for their biomedical and environmental applications.

REFERENCES

Abdullah et al. (2020). Green Synthesis and characterization of Iron oxide nanoparticles . *Sustainable Chemistry and Pharamacy*, 100280.

Adedapo.A et al. (2008). Antibacterial and antioxidant properties of the methanol extracts of the leaves and stems of Calpurnia aurea. *BMC Complement Altern Med 8*, 1472-6882-8-53.

Ahmad.S et al. (2014). Synthesis of iron oxide–tin oxide nanoparticles and evaluation of their activities. *Canadian Chemical Transactions, 2*, 122-133.

Anamika et al. (2020). Adsorption study of Heavy Metals from Aqueous Solutions using Magnetite Nanoparticles. *Journal of Physics Conference Series Conf. Ser. 1504 012011*, 1-13.

Ankamwar et al. (2005). Biosynthesis of gold and silver nanoparticles using emblica officinalis fruit extract, their phase transfer and transmetallation in an organic solution. *J. Nanosci Nanotechnol.*, 5(10):1665-71.

Arakha et al. (2015). Antimicrobial activity iron oxide nano particles upon modulation of nano particle-bacteria interface . *Scientific reports*, 14813.

Arap W et al. (1998). Cancer treatment by targeted drug delivery to tumor vasculature in amouse model. *Sci. 279(5349)*, 377-80.

Araujo.R et al. (2021). Hybrid hematite/calcium ferrite fibers by solution blow spinning:Microstructural, optical and magnetic characterization. *Ceramics International 47* , 1-19

Arivalagan.K et al. (2011). Nanomaterials and its potential applications. *Int. J. ChemTech Res. 3*,534.

Arokiyaraj et al. (2013). Enhanced antibacterial activity of iron oxide magnetic nanoparticles treated with Argemone Mexicana L. leaf extract. *An in vitro study.Materials Research Bulletin, 48(9)*, 3323–3327.

Arpan.B et al. (2015). "Modelling Size and Structure of Nanoparticles Formed from Drying of Submicron Solution Aerosols. *JOURNAL OF NANOPARTICLE RESEARCH*, 1-9.

Azam et al. (2012). Size-dependent antimicrobial properties of CuO nanoparticles against Gram-positive and -negative bacterial strains. *Int J Nanomedicine.* , 3527–3535.

Balouiri.M et al. (2016). Methods for in vitro evaluating antimicrobial activity. *A review. J Pharm Anal.*, 71-79.

Bauer et al. (1966). Antibiotic susceptibility testing by a standardized single disk method. . *Tech Bull Regist Med Technol.*, 49-52.

Bonzkurt.G. (2020). Synthesis and Characterization of α-Fe2O3 Nanoparticles by Microemulsion Method. *Journal of Science and Technology 13(2),*, 890-897.

Campos E.A et al. (2015). Synthesis, Characterization and Applications of Iron Oxide Nanoparticles – a Short Review. *J. Aerosp. Technol. Manag.*, 267-276.

Chang et al. (2023). Physical mechanism of electrode coatings to suppress wire particle‟s firefly motion under DC stress and selecting criterion for in situ applications. *Physica Scripta*, 1-7.

Chatzimitakos et al. (2016). Antibacterial, anti-biofouling, and antioxidant prospects of metal-based nanomaterials. . *CLEAN Soil Air Water.*, 794–802.

Chen et al. (2009). Platinum-Doped TiO2/Magnetic Poly (methyl methacrylate) Microspheres as a Novel Photocatalyst. . *Ind. Eng. Chem. Res., Volume 48*, p. 7616–7623.

Cheng et al. (2013). Synthesis and antibacterial effects of aqueous colloidal solutions of silver nanoparticles using aminocellulose as a combined reducing and capping reagent. *GreenChemistry,vol. 15(4)*, pp. 989–998.

Chung et al. (2004). In vivo cancer targeting and imaging with semiconductor quantum dots. *Nature biotechnology*, 969-976.

Cornell and Schwertmann. (2003). The Iron Oixdes: Structures, Properties,Reactions, and Occurences used. *Weinheim: Wiley*.

Cornell and Schwertmann. (2003). The Iron Oixdes: Structures, Properties,Reactions, and Occurences used. *(Weinheim: Wiley).*

Duan and Guojun. (2005). introduction to condensed physics. *ISBN*, 13.

Dwivedi.P et al. (2024). Eco-Friendly CuO/Fe3O4 Nanocomposite synthesis, characterization, and cytotoxicity study. *Heliyon 10* , 1-10.

Eiglesias.S et.al. (2007). Synthesis of Silver Coated Magnetic Nano- particles. *Journal of Non Crystal Solids, 353,*, 829-831.

Estelrich et al. (2015). Nanoparticles in Magnetic Resonance Imaging. *International Journal of Nanomedicine*, 1727-1741.

Faller et al. (2004). Determination of fungicidal activities against yeasts and molds: lessons learned from bactericidal testing and the need for standardization. *Clin. Microbiol.* , 268–280.

Fang.Q et al. (2011). Porous Metal–Organic Frameworks. *Comprehensive Nanoscience and Technology*, 1-20.

Fardood S.T et al. (2017). Green Synthesis of α-Fe2O3 (hematite) Nanoparticles using Tragacanth Gel. *Journal of Applied Chemical Research, 11, 3, ,* 19-27.

Figuerola et al. (2010). From iron oxide nanoparticles towards advanced iron-based inorganic materials designed for biomedical applications, Pharmacol,. *Res. 62*, 126- 143.

Gabrielyan et al. (2021). Antibacterial activity of royal jelly-mediated green synthesized silver nanoparticles. *AMB Express*, 1-8.

Gajic et al. (2022). Antimicrobial Susceptibility Testing: A Comprehensive Review of Currently Used Methods. *Antibiotics*, 427.

Ganachari et al. (2019). Metal oxide nanomaterials for environmental applications. *Handbook of Ecomaterials*, 2357-2368.

Gebreslassie.Y et al. (2023). Biomedical Applications of Biosynthesized Nickel Oxide Nanoparticles. *International Journal of Nanomedicine*, 4229–4251.

Geneti S.T et al. (2022). Biogenic Synthesis of Magnetite Nanoparticles Using Leaf Extract of Thymus schimperi and Their Application for Monocomponent Removal of Chromium and Mercury Ions from Aqueous Solution. *ournal of Nanomaterials Volume 2022*, 1-16.

Gogoi et al. (2022). Nanostructured Iron Oxide Hybrid Composites as Heterogeneous Fenton-Like Catalyst for Remediation of Persistent Organic Pollutants. *Heterogeneous Nanocatalysis for Energy and Environmental Sustainability*, 37-71.

Gordon et al. (2011). Synthesis and characterization of zinc/iron oxide composite, Nanoparticles and their antibacterial properties, Colloids and Surfaces A. *Physicochemical and Engineering Aspects.*, 374(1): 1-8.

Gu et al. (2006). Biofunctional Magnetic Nanoparticles for Protein Separation and Pathogen Detection. *Chem. Commun. Volume 9*, 941- 949.

Gudkov.S et al. (2021). Do Iron Oxide Nanoparticles Have Significant Antibacterial Properties ? *Antibiotics (Basel, Switzerland)*, 884.

Gupta and Gupta. (2005). Synthesis and surface engineering of iron oxide nanoparticles for biomedical applications. *biomaterials*, 3995-4021.

Hajipour et al. (2012). Antibacterial properties of nanoparticles, Trend. *Biotechnol, 30(10).*, 499-511.

Hakim et al. (2023). Annealing Temperature Dependent of the Structural and Magnetic Properties in Hematite Prepared by Sol-Gel Method. *Engineering Materials*, 1-9.

Harraz et al. (2014). Magnetic nanocomposite based on titania– silica/cobalt ferrite for Photocatalytic degradation of methylene blue dye. *Ceramics International,Volume 40,*, p. 375–384.

Hill et al. (1979). Systematics of the spinel structure type. . *Physics and chemistry of minerals*, 317-339.

Hjiri et al. (2024). Gas sensing properties of hematite nanoparticles synthesized via different techniques. *RSC advances*, 17526-17534.

Hossein.P et al. (2015). Synthesis of ZnO Nanoparticles by Precipitation Method. *Department of Chemical Engineering*, 1-3.

Hufschmid et al. (2015). Synthesis of phase-pure and monodisperse iron oxide nanoparticles by thermal decomposition. *Nanoscale*, 11142- 11154.

Hui et al. (2008). Large scale Fe3O4 nanoparticles soluble in water synthesized by a facile method. *J. Phys. Chem*, 11336–11339.

Husain.H et al. (2018). Local structure examination of mineral-derived Fe2O3 powder by Fe K-edge EXAFS and XANES. *Materials Science and Engineering*, 367.Iravani .S et al. (2011). Green synthesis of metal nanoparticles using plants. . *Green Chemistry*, 2638-50.

Jeffrey et al. (2008). Performance Standards for Antimicrobial Disk and Dilution Susceptibility Tests for Bacteria Isolated from animals . *Approved Standard third edition, Clinical and Laboratory Standards Institute*, 28(8).

Jiang et al. (2008). Magnetic iron oxide nanoparticles: Synthesis and surface fictionalizations strategies, . *Nanoscale, Res. Lett. 3*, 397–415.

Kiwumulo H.F et al. (2022). Green synthesis and characterization of iron-oxide nanoparticles using Moringa oleifera: a potential protocol for use in low and middle income countries. *BMC Research Notes 15*, 1-8.

Kumar and Ananthu. (2018). Green Synthesis and Characterization of Iron Oxide Nanoparticles Using Phyllanthus Niruri Extract. *Oriental Journal of Chemistry* , 34.

Kurczewska.J and Dobosz.B. (2024). Recent Progress and Challenges Regarding MagnetiteBased Nanoparticles for Targeted Drug Delivery. *Appl. Sc*, 1132.

Lassoued.A et al. (2017). Control of the shape and size of iron oxide (a-Fe2O3) nanoparticles synthesized through the chemical precipitation method. *Results in Physics 7* , 3007–3015.

Laurent et al. (2008). Magnetic iron oxide nanoparticles: Synthesis, stabilization, vectorization,physicochemical characterizations, and biological applications. *Chemical Reviews,108(6)*, 2064–2110.

Lee et al. (2020). Effects of pH and reaction temperature on hydroxyapatite powders synthesized by precipitation. *J. Korean Ceram. Soc. 57*, 56–64.

Li .Y et al. (2012). In vitro biological effects of magnetic nanoparticles . *Chinese Science Bulletin*, 3972–3978.

Liu et al. (2021). Construction of homologous cancer cell membrane camouflage in a nano-drug delivery system for the treatment of lymphoma. *Nanobiotechnology*, 1-19.

M.Getachew. (2020). Antibacterial activity of C.aurea against selected animal pathogenic Bacterial strains. *Adv Pharmacol Pharm Sci*, 8840468.

Malik.S et al. (2023). Nanotechnology: A Revolution in Modern Industry . *Molecules. 2023 Jan*, 1-26.

Masalha et al. (2001). Analysis of transcription of the staphylococcus aureus aerobics class Ib and anaerobic class III ribonucleotides reductase genes in response to oxygen. . *Journal of Bacteriology.*, 183(24) 7260-7272.

Materon et al. (2021). Magnetic nanoparticles in biomedical applications. *Applied Surface Science*, 100163.

Mishra et al. (2008). Effect of yttrium on improvement of dielectric properties and magnetic switching behavior in BiFeO3. *Journal of Physics:*, 045218.

Mohamed.M et al. (2023). Green synthesis and characterization of iron oxide nanoparticles for the removal of heavy metals (Cd2+ and Ni2+) from aqueous solutions with Antimicrobial Investigation. *Scientific Reports 13:7227*, 1-30.

Nalbandian.L et al. (2015). Magnetic Nanoparticles in Medical Diagnostic Applications: Synthesis, Characterization and Proteins Conjugation. *Current Nanoscience 12*, 1-26.

Navio et al. (2010). Formation of zirconium Titanate powder from a Sol-gel prepared reactive precursor. . *J. Mater. Sci*, 27,2463.

Ndou.N et al. (2023). Green Synthesis of Iron Oxide (Hematite) Nanoparticles and Their Influence on Sorghum bicolor Growth under Drought Stress. *plants12071425*, 1-23.

Nguyen M.D et al. (2021). Fe3O4 Nanoparticles: Structures, Synthesis, Magnetic Properties, Surface Functionalization, and Emerging Applications. *Appl. Sci 11*, 11301.

Nurbaş. M et al. (2017). An Eco-friendly Approach to Synthesis and Characterization of Magnetite (Fe3O4) Nanoparticles Using Platanus Orientalis L. Leaf Extract VL-12. *Digest Journal of Nanomaterials and Biostructures*, 993-1000.

Pandey et al. (2023). Comparing the Variants of Iron Oxide Nanoparticle-Mediated Delivery of miRNA34a for Efficiency in Silencing of PD-L1 Genes in Cancer Cells. *Pharmaceutics*, 15, 215.

Pang.Z et al. (2019). Antibiotic resistance in Pseudomonas Aeruginosa: Mechanisms and alternative therapeutic strategies. . *Biotechnol. Adv*, 177–192.

Parhizkar.J, Habibi M.H. (2017). Synthesis, characterization and photocatalytic properties of Iron oxide nanoparticles synthesized by sol-gel autocombustion with ultrasonic irradiation. *Nanochem Res 2(2)*, 166-171.

Rafael.A et al. (2023). Green Synthesis of Nanoparticles: A Biological Approach. *Advances in Green Chemistry*, 1-18.

Raghunath A and Perumal . (2017). Metal oxide nanoparticles as antimicrobial agents: . *a promise for the future. ijantimicag. 49:137-152. https://doi.org/10.1016/j. ijantimicag*, 11.011.

Rivero K.T et al. (2021). Metal and metal oxide nanoparticles: An integrated perspective of the green synthesis methods by natural products and waste valorization: applications and challenges. *Comprehensive Analytical Chemistry Volume 94*, 433-469.

Rufus.A. (2017). Biosynthesis of hematite (α-Fe2O3) nanostructures: Size effects on applications in thermal conductivity, catalysis, and . *Journal of Molecular Liquids*.

Sahoo et al. (2011). Role of the Inflammasome, IL-1 , and IL- 18 in Bacterial Infections. *The Scientific World Journal*, 2037-2050.

Saqib.S et al. (2018). Synthesis characterization and use of iron oxide nanoparticles for antibacterial activity. *Microsc Res Tech*, 1–6.

Seil and Webster. (2012). Antimicrobial applications of nanotechnology: methods and literature. *International journal of nanomedicine*, 2767-2781.

Shah M et al. (2015). Green synthesis of metallic nanoparticles via biological entities. *Materials, 8 (11)*, 7278–7308.

Shariatzadeh et al. (2022). Nanostructured α-Fe2O3: Solvothermal Synthesis, Characterization, and Effect of Synthesis Parameters on Structural Properties. *International Journal of Engineering Vol. 35, No. 06,*, 1186-1192.

Singh et al. (2014). The role of nanotechnology in combating multi-drug resistant bacteria. *J. Nanosci. Nanotechnol, 14(7),* 4745–4756.

Sportelli et al. (2016). Investigation of industrial polyurethane foams modified with antimicrobial copper nanoparticles. *Materials, 9(7):* , 544.

Tadeg.H et al. (2005). Antimicrobial activities of some selected Traditional Ethiopian medicinal plants used in the treatment of skin disorders. *J Ethno pharmacol,* 100:168-175.

Taib N.I et al. (2018). Green Synthesis of Iron Oxide Nanoparticles (Fe3O4-NPs) using Azadirachta Indica Aqueous Leaf Extract. *International Journal of Engineering & Technology, 7 (4.18)* , 9-13.

Tartaj et al. (2003). The preparation of magnetic nanoparticles for applications in biomedicine. . *J. Phys D: Appl Phys. 36:,* 182-197.

Thakkar K.N et al. (2010). Biological synthesis of metallic nanoparticles. *Nanomedicine, 6(2),* 257–262.

Upadhyay et al, .. (2016). Influence of crystallite size on the magnetic properties of Fe3O4 nanoparticles. *Journal of Alloys and Compounds 678,* 478-485.

Urvashi Kheskwani and M. Mansoor Ahammed. (2023). Removal of water pollutants using plant-based nanoscale zero-valent iron: A review. *Water Science & Technology Vol 88 No 5, 1207* , 1-25.

Valášková.M et al. (2019). α-Fe2O3 Nanoparticles/Vermiculite Clay Material:Structural, Optical and Photocatalytic Properties. *Materials, 12,1880,* 1-16.

Valladares D.L et al. (2019). Characterization and magnetic properties of hollow a-Fe2O3 microspheres obtained by sol gel and spray roasting methods. *Journal of Science: Advanced Materials and Devices 4,* 483-491.

Vicky et al. (2010). Introduction to metallic nanoparticles, J. Pharm. *Bioallied Sci. 2(4),* 282-289.

Wang.L et al. (2017). The antimicrobial activity of nanoparticles : Present situation and prospects for the future. *International Journal of Nanomedicine, 12,* 1227–1249.

Woolhouse et al. (2015). Antimicrobial resistance in humans, livestock and the wider environment, . *Philosophical Transactions of the Royal Society B.,* 1670).

Wu et al. (2010). Large-scale and controlled synthesis of iron oxide magnetic short nanotubes: shape evolution, growth mechanism, and magnetic properties. *J. Phys.Chem. C. 114:*, 16092.

Xu Zong, Can Li. (355-399). 2018. *Metal Oxides in Heterogeneous Catalysis*, 1-16.

Xu.P et al. (2012). Use of iron oxide nanomaterials in wastewater treatment: A review. *Science of The Total Environment Volume 424*, 1- 10.

Yamamoto et al. (2001). Influence of particle size on the antibacterial activity of zinc oxide. *Int J. Inorg. Mater, 3(7),* 643–646.

Yang L et al. (2008). Development of receptor targeted magnetic iron oxide nanoparticles for efficient drug delivery and tumor imaging, J. Biomed. *Nanotechnol, 4*, 439.

Yetter et al. (2009). Effect of particle size on combustion of aluminum particle dust in air. *Combustion and Flame*, 5-13.

Yineger H et al. (2008). Ethnomedicinal plant knowledge and practice of the Oromo ethnic group in southwestern Ethiopia. . *J. Ethnobiol. Ethnomed.* , 4:11-21.

Zhou et al. (2009). Electrochemical Characterization of Li3N–Si Nanocomposite Thin Films by

Pulsed Laser Deposition. *Journal of the Electrochemical Society.*, 425.

Appendix

Table 3: Antibacterial Activity of Fe_2O_3 Nps and Fe_3O_4 Nps

SN	Sample Name	Conc.mg/ml	Inhibition zone in mm (mean ± standard deviation)			
			S. aureus	S. pyogenes	E. coli	P. aeruginosa
1	1:1 Fe_2O_3	300 (1)	10.33±0.47	8.33±0.47	8.67±0.47	8.67±0.94
		150 (2)	7.67±0.47	7.33±0.47	8.00±0.00	8.67±0.47
		75 (3)	7.33±0.47	7.00±0.81	7.33±1.24	8.00±0.81
		37.5 (4)	7.00±0.81	6.67±0.47	7.00±0.81	7.67±0.94
		18.75 (5)	6.67±0.94	6.33±0.47	7.00±0.81	7.34±0.94
		30 µg/ml (+Ve)	21.33±1.24	20.00±0.81	20.66±1.24	21.33±1.24
2	1:2 Fe_2O_3	300 (1)	10.33±0.81	10.00±0.81	9.67±0.47	10.00±0.81
		150 (2)	10.00±0.81	9.67±0.47	9.33±0.47	9.67±0.47
		75 (3)	9.67±0.47	9.33±.0.47	9.00±0.81	9.34±0.47
		37.5 (4)	8.67±0.47	9.00±0.47	8.00±0.81	8.34±1.24
		18.75 (5)	7.67±0.47	7.34±1.24	7.67±0.94	7.67±0.94
		30 µg/ml (+Ve)	22.00±0.81	19.34±0.47	20.00±0.81	19.34±0.47
3	2:1 Fe_2O_3	300 (1)	10.34±0.94	10.00±0.81	9.67±0.47	10.33±0.47
		150 (2)	9.67±0.47	9.34±0.47	9.34±0.47	10.00±0.00
		75 (3)	9.34±0.47	8.34±0.94	8.66±0.94	9.34±0.47
		37.5 (4)	8.34±0.47	8.00±0.81	8.34±0.94	8.66±0.47
		18.75 (5)	8.00±0.81	7.34±0.47	7.33±0.94	8.00±0.81
		30 µg/ml (+Ve)	21.00±0.81	18.67±0.94	19.34±0.47	20.34±0.47
4	1:1 Fe_3O_4	300 (1)	9.00±1.41	8.67±0.47	9.34±0.47	10..34±0.47
		150 (2)	8.34±0.94	8.34±0.47	8.33±0.47	8.67±0.47
		75 (3)	7.67±1.24	7.67±0.94	7.00±0.81	7.34±0.47
		37.5 (4)	7.00±0.81	7.00±0.81	6.66±0.47	6.67±0.47
		18.75 (5)	6.67±0.94	6.67±0.47	6.34±0.47	6.34±0.47
		30 µg/ml (+Ve)	28.33±1.24	21.00±1.63	21.67±0.94	20.34±0.47
5	1:2 Fe_3O_4	300 (1)	8.67±0.47	9.34±0.47	8..34±0.47	9.34±0.47
		150 (2)	8.00±0.81	8.34±0.47	8.00±0.81	9.00±0.00
		75 (3)	7.00±0.81	8.00±0.81	7.67±0.47	8.33±0.47
		37.5 (4)	6.67±0.94	7.34±1.24	7.34±0.47	8.00±0.81
		18.75 (5)	6.34±0.47	7.00±0.00	7.00±0.81	7.34±0.47
		30 µg/ml (+Ve)	20.67±1.24	18.67±1.69	19.34±1.24	20.34±1.88
6	2:1 Fe_3O_4	300 (1)	8.34±1.24	9.34±0.47	10.00±0.81	10.67±0.94
		150 (2)	7.34±1.24	8.34±0.47	9.67±0.94	10.34±0.47
		75 (3)	6.67±0.94	8.00±0.81	9.00±1.41	9.34±0.47
		37.5 (4)	6.34±0.47	7.34±0.47	7.66±0.94	9.00±0.81
		18.75 (5)	6.00±0.00	6.67±0.47	6.67±0.94	8.67±0.47
		30 µg/ml (+Ve)	21.67±0.47	22.67±1.24	22.00±0.81	20.67±0.94